

Initialization of Homoclinic Solutions near Bogdanov–Takens Points: Lindstedt–Poincaré Compared with Regular Perturbation Method*

B. Al-Hdaibat[†], W. Govaerts[‡], Yu. A. Kuznetsov[‡], and H. G. E. Meijer[§]

Abstract. To continue a branch of homoclinic solutions starting from a Bogdanov–Takens (BT) point in parameter and state space, one needs a predictor based on asymptotics for the bifurcation parameter values and the corresponding small homoclinic orbits in the phase space. We derive two explicit asymptotics for the homoclinic orbits near a generic BT point. A recent generalization of the Lindstedt–Poincaré (L-P) method is applied to approximate a homoclinic solution of a strongly nonlinear autonomous system that results from blowing up the BT normal form. This solution allows us to derive an accurate second-order homoclinic predictor to the homoclinic branch rooted at a generic BT point of an n -dimensional ordinary differential equation (ODE). We prove that the method leads to the same homoclinicity conditions as the classical Melnikov technique, the branching method, and the regular perturbation (R-P) method. However, it is known that the R-P method leads to a “parasitic turn” near the saddle point. The new asymptotics based on the L-P method do not have this turn, making them more suitable for numerical implementation. We show how to use these asymptotics to calculate the initial data to continue homoclinic orbits in two free parameters. The new homoclinic predictors are implemented in the MATLAB continuation package MatCont to initialize the continuation of homoclinic orbits from a BT point. Two examples with multidimensional state spaces are included.

Key words. Bogdanov–Takens bifurcation, homoclinic orbits, Lindstedt–Poincaré method, regular perturbation method, MatCont

AMS subject classifications. 34C20, 34E10, 37G20, 37M20, 65L07

DOI. 10.1137/15M1017491

1. Introduction. A generic Bogdanov–Takens (BT) point is the root in parameter space of branches of fold, Andronov–Hopf, and homoclinic-to-saddle bifurcations. Many techniques have been developed to continue these curves starting from a BT point [34, 5, 29, 30]. It is well known that the BT point is a regular point for the continuation problem of the fold curve as well as of the Hopf curve (that is, if the Hopf curve is defined by requiring that there be two eigenvalues summing up to zero). The difficult task is to continue homoclinic orbits starting from a BT point where the homoclinic orbits shrink to the equilibrium while tracing the homoclinic bifurcation curve. In this case, the problem is regular near the BT point but

*Received by the editors May 4, 2015; accepted for publication (in revised form) by D. Barkley November 30, 2015; published electronically May 17, 2016.

<http://www.siam.org/journals/siads/15-2/M101749.html>

[†]Department of Applied Mathematics and Computer Science, Ghent University, Krijgslaan 281-S9, B-9000, Ghent, Belgium (Bashir.AIHdaibat@UGent.be, WillyGovaerts@UGent.be). The first author was supported by the Hashemite University in Jordan during his Ph.D. research at Ghent University.

[‡]Department of Mathematics, Utrecht University, Budapestlaan 6, 3508 TA Utrecht, The Netherlands, and Department of Applied Mathematics, University of Twente, 7500AE Enschede, The Netherlands (I.A.Kouznetsov@uu.nl).

[§]Department of Applied Mathematics, University of Twente, 7500AE Enschede, The Netherlands (H.G.E.Meijer@utwente.nl).

not at the BT point itself, so that a small nonzero step away from the BT point is required. One therefore needs a special predictor based on asymptotics for the bifurcating parameter values and the corresponding small homoclinic orbits in the phase space. These predictors should be constructed in the normal form system for the BT bifurcation by performing a singular rescaling that brings the normal form into a Hamiltonian system (with an explicit homoclinic solution) plus a small perturbation depending on parameter $\varepsilon \ll 1$. In this case the classical Melnikov method [26] or the equivalent branching method [5] has been used to derive a first-order approximation for the homoclinic bifurcation curve in parameter space and the zero-order approximation for the homoclinic orbit in phase space, and the regular perturbation (R-P) method [29, 30] has been used as well to derive the second-order approximation for these solutions both in the parameter and the phase space. Here and in what follows, the order of predictor refers to the maximal order in the ε -expansion of the homoclinic solution in the perturbed Hamiltonian systems, and not to the truncation ε -order in the final predictors.

The idea of starting homoclinic orbits near a BT point in planar systems with the help of Melnikov's method was developed by Rodriguez, Freire, and Ponce [34]. Beyn [5] treated the general n -dimensional problem. He derived the first asymptotics, i.e., a *homoclinic predictor*, of the homoclinic solutions near a generic BT point. These asymptotics were initially derived for the normal form system. Then, using the parameter-dependent center manifold reduction, the asymptotics were lifted to the phase and parameter spaces of the original n -dimensional system. Kuznetsov et al. [29] improved these asymptotics by correcting the parameter transformation presented in [5, 6] and by deriving an explicit first-order correction of the homoclinic orbit and the corresponding parameter values. They applied the R-P method to derive such asymptotics for the topological normal form used in [26, 16, 39]. In [30], a second-order correction for the homoclinic bifurcation curve is derived. This predictor depends on some terms of the two-dimensional (2D) smooth normal form which do not appear in the topological normal form. However, the approximation of the homoclinic solution by the R-P method always involves a "parasitic turn" near the saddle point. Actually, as the perturbation parameter ε increases, the $\mathcal{O}(\varepsilon)$ -corrections quickly become larger than the zero-order approximation, and then the expansion breaks down for large times.

Chen et al. [10, 14, 13, 11, 15] used a generalization of the Lindstedt–Poincaré (L-P) method to study the homoclinic solution to a family of nonlinear oscillators. They applied a nonlinear transformation of time instead of the linear one used in the original L-P method for periodic solutions (see, e.g., [33] for the original L-P method). Belhaq, Fiedler, and Lakrad [4] proved that the generalized L-P method combined with a special criterion leads to the same results as the classical Melnikov technique. This criterion is based on a collision between the bifurcating limit cycle near the homoclinic orbits with a saddle equilibrium point. They proved that this *collision criterion* is equivalent to the vanishing distance between the separatrices in the Melnikov technique. We should also point out that yet another approach based on periodic time transformations exists in the literature [8]. However, the L-P method has a clear advantage since it provides an explicit time-parametrization which is necessary for numerical continuation.

In the present paper, we compare two homoclinic predictors near a generic codim 2 BT point. The L-P method is used for approximating homoclinic solutions of a family of strongly

nonlinear autonomous systems,

$$\ddot{u} - u^2 + 4 = \varepsilon f(\dot{u}, u, \tau, \varepsilon),$$

that result from blowing up the BT normal form. We show how the L-P method leads to the same homoclinicity conditions as the Melnikov technique, the branching method, and the R-P method. The derived predictor does not have a “parasitic turn” near the saddle point. This improves the prediction in the phase space. A numerical comparison illustrating the results is presented. The new homoclinic solution allows us to derive an accurate second-order homoclinic predictor of the homoclinic bifurcation for a general n -dimensional system. We also show how these asymptotics can be used to calculate the initial homoclinic solution to continue homoclinic orbits in two free parameters. The new homoclinic predictor is implemented in the MATLAB continuation package MatCont [20, 21] to initialize the continuation of homoclinic orbits from a BT point in multidimensional models.

The paper is organized as follows. Section 2 is a brief recollection of necessary normal form and center manifold results. Using an appropriate smooth BT normal form, the parameter-dependent center manifold reduction is described and the BT normal form coefficients are computed. In section 3, we use the R-P method to derive explicitly a third-order correction for the homoclinic solutions to the BT normal form system. Then the L-P method is used to solve the same problem and to derive a third-order correction to the homoclinic solution. We prove that the L-P method leads to the same homoclinicity conditions. A numerical comparison is presented to illustrate the accuracy of the asymptotics for both methods. Section 4 combines the results obtained from the previous sections and provides the explicit formulas for the second-order homoclinic predictors. In section 5, we describe the exact algorithm used in MatCont to initialize the homoclinic continuation from a BT point. Numerical examples with MatCont are presented in section 6.

2. Smooth normal form on the parameter-dependent center manifold. Suppose that at $(x_0, \alpha_0) = (0, 0)$ the Jacobian matrix $A = f_x(x_0, \alpha_0)$ of a generic smooth family of autonomous ordinary differential equations (ODEs),

$$(1) \quad \dot{x} = f(x, \alpha), \quad f : \mathbb{R}^n \times \mathbb{R}^2 \rightarrow \mathbb{R}^n,$$

has a double (but not semisimple) zero eigenvalue, i.e., (x_0, α_0) is a BT point. Then there exist two real linearly independent (generalized) eigenvectors $q_{0,1} \in \mathbb{R}^n$, of A , and two adjoint eigenvectors $p_{0,1} \in \mathbb{R}^n$, of A^T , such that

$$(2) \quad \begin{pmatrix} A & 0 \\ -I_n & A \end{pmatrix} \begin{pmatrix} q_0 \\ q_1 \end{pmatrix} = 0, \quad \begin{pmatrix} A^T & 0 \\ -I_n & A^T \end{pmatrix} \begin{pmatrix} p_1 \\ p_0 \end{pmatrix} = 0.$$

We can assume that the vectors satisfy

$$(3) \quad p_0^T q_0 = p_1^T q_1 = 1, \quad p_0^T q_1 = p_1^T q_0 = 0.$$

If we further impose the conditions [28]

$$(4) \quad q_0^T q_0 = 1, \quad q_1^T q_0 = 0,$$

then the vectors $\{q_0, q_1, p_0, p_1\}$ are uniquely defined up to a \pm sign. The smooth normal form for the restriction of a generic system (1) to its parameter-dependent 2D center manifold near the BT bifurcation is

$$(5) \quad \dot{w} = G(w, \beta) = \begin{pmatrix} w_1 \\ \beta_1 + \beta_2 w_1 + a w_0^2 + b w_0 w_1 + g(w, \beta_2) \end{pmatrix} \\ + \mathcal{O}(|\beta_1| \|w\|^2 + |\beta_2| w_1^2) + \mathcal{O}(\|\beta\|^2 \|w\|^2 + \|\beta\| \|w\|^3 + \|w\|^4),$$

where $g(w, \beta_2) := a_1 \beta_2 w_0^2 + b_1 \beta_2 w_0 w_1 + d w_0^3 + e w_0^2 w_1$. Here $w = (w_0, w_1) \in \mathbb{R}^2$ parametrizes the 2D parameter-dependent center manifold of (1), and $\beta = (\beta_1, \beta_2) \in \mathbb{R}^2$ are the unfolding parameters, while a, a_1, b, b_1, d , and e are the normal form coefficients. Truncating the \mathcal{O} -terms and omitting $g(w, \beta_2)$ gives the well-known topological normal form for the BT bifurcation (see, e.g., [1, 26]),

$$(6) \quad \dot{w} = \begin{pmatrix} w_1 \\ \beta_1 + \beta_2 w_1 + a w_0^2 + b w_0 w_1 \end{pmatrix},$$

where as a nondegeneracy condition it is assumed that $ab \neq 0$. We emphasize that it is essential to include the term $g(w, \beta_2)$ in addition to the topological normal form to achieve an accurate second-order approximation for the homoclinic solution of (1) which depends on the term $g(w, \beta_2)$ [30]. This term was ignored in earlier studies [5, 29].

Suppose that an explicit approximate homoclinic for the normal form (5) is available. In order to transfer this back to the original system (1) we need a relation

$$(7) \quad \alpha = K(\beta), \quad K: \mathbb{R}^2 \rightarrow \mathbb{R}^2,$$

between the unfolding parameters β and the original system parameter α . Moreover, we need to parametrize the center manifold for (1) by (w, β) ,

$$(8) \quad x = H(w, \beta), \quad H: \mathbb{R}^2 \times \mathbb{R}^2 \rightarrow \mathbb{R}^n.$$

Taking (7) and (8) together as $(x, \alpha) = (H(w, \beta), K(\beta))$ yields the center manifold for the suspended system

$$\begin{cases} \dot{x} = f(x, \alpha), \\ \dot{\alpha} = 0. \end{cases}$$

The invariance of the center manifold implies the *homological equation*

$$(9) \quad H_w(w, \beta) G(w, \beta) = f(H(w, \beta), K(\beta)).$$

We write the Taylor expansions of K , H , and f as

$$(10a) \quad f(x, \alpha) = Ax + J_1\alpha + \frac{1}{2}B(x, x) + A_1(x, \alpha) + \frac{1}{2}J_2(\alpha, \alpha) + \frac{1}{6}C(x, x, x) + \frac{1}{2}B_1(x, x, \alpha) \\ + \mathcal{O}(\|x\|\|\alpha\|^2 + \|\alpha\|^3) + \mathcal{O}(\|(x, \alpha)\|^4),$$

$$(10b) \quad H(w, \beta) = q_0w_0 + q_1w_1 + H_{0010}\beta_1 + H_{0001}\beta_2 + \frac{1}{2}H_{2000}w_0^2 + H_{1100}w_0w_1 + \frac{1}{2}H_{0200}w_1^2 \\ + H_{1010}\beta_1w_0 + H_{1001}\beta_2w_0 + H_{0110}\beta_1w_1 + H_{0101}\beta_2w_1 + \frac{1}{2}H_{0002}\beta_2^2 + \frac{1}{6}H_{3000}w_0^3 \\ + \frac{1}{2}H_{2100}w_0^2w_1 + \frac{1}{2}H_{2001}\beta_2w_0^2 + H_{1101}\beta_2w_0w_1 + \mathcal{O}(\beta_1^2 + |\beta_1\beta_2|) \\ + \mathcal{O}(|w_1|^3 + |w_0w_1^2| + |\beta_2w_1^2| + |\beta_1\|w\|^2 + \|\beta\|^2\|w\| + \|\beta\|^3) + \mathcal{O}(\|(w, \beta)\|^4),$$

$$(10c) \quad K(\beta) = K_{1,0}\beta_1 + K_{1,1}\beta_2 + \frac{1}{2}K_2\beta_2^2 + \mathcal{O}(\beta_1^2 + |\beta_1\beta_2|) + \mathcal{O}(\|\beta\|^3),$$

where $A = f_x(x_0, \alpha_0)$, $J_1 = f_\alpha(x_0, \alpha_0)$, and B , A_1 , J_2 , C , B_1 are the standard multilinear forms.

We insert the expansions (10a)–(10c) into (9) together with the normal form (5). Then the resulting equations for terms of the same order in w and β can be solved by a recursive procedure based on Fredholm's solvability condition that gives the Taylor coefficients of H and K , as well as the coefficients a, a_1, b, b_1, d , and e of the normal form. The linear and quadratic (w, β) -terms in the homological equation lead to

$$(11) \quad a = \frac{1}{2}p_1^T B(q_0, q_0),$$

$$(12) \quad b = p_0^T B(q_0, q_0) + p_1^T B(q_0, q_1),$$

$$(13) \quad H_{2000} = A^{\text{INV}}(2aq_1 - B(q_0, q_0)) + \gamma q_0,$$

$$(14) \quad H_{1100} = A^{\text{INV}}(bq_1 + H_{2000} - B(q_0, q_1)),$$

$$(15) \quad H_{0200} = A^{\text{INV}}(2H_{1100} - B(q_1, q_1)),$$

where

$$\gamma := \frac{1}{2}(-2p_0^T H_{2000} + 2p_0^T B(q_0, q_1) + p_1^T B(q_1, q_1)).$$

Note that γq_0 is added to H_{2000} to ensure that the right-hand side (R.H.S.) of the system for H_{0200} is in the range of A ; see [27, section 8.7] for more details. Moreover, the vectors H_{0010} , H_{0001} , $K_{1,0}$, and $K_{1,1}$ can be computed by solving the $(n+2)$ -dimensional system as described in [29]:

$$(16) \quad \begin{pmatrix} A & J_1 \\ p_1^T B q_0 & p_1^T A_1 q_0 \\ p_0^T B q_0 + p_1^T B q_1 & p_0^T A_1 q_0 + p_1^T A_1 q_1 \end{pmatrix} \begin{pmatrix} H_{0010} & H_{0001} \\ K_{1,0} & K_{1,1} \end{pmatrix} = \begin{pmatrix} q_1 & 0 \\ \frac{1}{2}p_1^T B(q_1, q_1) & 0 \\ c & 1 \end{pmatrix},$$

where $c := 3p_0^T H_{1100} - p_0^T B(q_1, q_1)$. The nonsingularity of this system is equivalent to the above-mentioned genericity condition for the validity of the smooth normal form (5). As soon as K_1 and H_{01} are determined, we can solve the following systems:

$$(17) \quad K_2 = -\left(p_1^T (B(H_{0001}, H_{0001}) + 2A_1(H_{0001}, K_{1,1}) + J_2(K_{1,1}, K_{1,1}))\right) K_{1,0},$$

$$(18) \quad H_{0002} = -A^{\text{INV}} (B(H_{0001}, H_{0001}) + 2A_1(H_{0001}, K_{1,1}) + J_2(K_{1,1}, K_{1,1}) + J_1 K_2),$$

$$(19) \quad H_{1001} = -A^{\text{INV}} (B(q_0, H_{0001}) + A_1(q_0, K_{1,1})),$$

$$(20) \quad H_{0101} = -A^{\text{INV}} (B(q_1, H_{0001}) + A_1(q_1, K_{1,1}) - H_{1001} - q_1)$$

(see [6, 29]). The homological equation then implies the following expressions for the cubic coefficients [30]:

$$(21) \quad d = \frac{1}{6} p_1^T (C(q_0, q_0, q_0) + 3B(q_0, H_{2000}) - 6aH_{1100}),$$

$$(22) \quad H_{3000} = -A^{\text{INV}} (C(q_0, q_0, q_0) + 3B(q_0, H_{2000}) - 6aH_{1100} - 6dq_1),$$

$$(23) \quad e = \frac{1}{2} p_1^T (C(q_0, q_0, q_1) + 2B(q_0, H_{1100}) + B(q_1, H_{2000}) - 2bH_{1100} - 2aH_{0200} - H_{3000}),$$

$$(24) \quad a_1 = \frac{1}{2} p_1^T (C(q_0, q_0, H_{0001}) + B_1(q_0, q_0, K_{1,1}) + 2B(q_0, H_{1001}) + B(H_{0001}, H_{2000}) + A_1(H_{2000}, K_{1,1}) - 2aH_{0101}),$$

$$(25) \quad H_{2001} = -A^{\text{INV}} (C(q_0, q_0, H_{0001}) + B_1(q_0, q_0, K_{1,1}) + 2B(q_0, H_{1001}) + B(H_{0001}, H_{2000}) + A_1(H_{2000}, K_{1,1}) - 2aH_{0101} - 2a_1 q_1),$$

$$(26) \quad b_1 = p_1^T (C(q_0, q_1, H_{0001}) + B_1(q_0, q_1, K_{1,1}) + B(q_1, H_{1001}) + B(H_{0001}, H_{1100}) + B(q_0, H_{0101}) + A_1(H_{1100}, K_{1,1}) - bH_{0101} - H_{1100} - H_{2001}).$$

In systems (13)–(15), (18)–(20), (22), and (25), the expression $x = A^{\text{INV}} y$ is defined by solving the nonsingular bordered system

$$\begin{pmatrix} A & p_1 \\ q_0^T & 0 \end{pmatrix} \begin{pmatrix} x \\ s \end{pmatrix} = \begin{pmatrix} y \\ 0 \end{pmatrix},$$

where y is in the range of A .

3. Homoclinic asymptotic in the smooth normal form. To construct an approximation for the homoclinic solution of (5), one first performs a blow-up transformation. We take the normal form (5) and apply the rescaling transformation

$$(27) \quad \beta_1 = -\frac{4}{a}\varepsilon^4, \quad \beta_2 = \frac{b}{a}\varepsilon^2\tau, \quad w_0 = \frac{\varepsilon^2}{a}u, \quad w_1 = \frac{\varepsilon^3}{a}v, \quad \varepsilon t = s;$$

cf. [26]. This transformation gives

$$\begin{cases} \dot{u} = v, \\ \dot{v} = -4 + u^2 + \varepsilon \frac{b}{a} v (\tau + u) + \varepsilon^2 \frac{1}{a^2} u^2 (\tau b a_1 + du) + \varepsilon^3 \frac{1}{a^2} uv (\tau b b_1 + eu) + \mathcal{O}(\varepsilon^4) \end{cases}$$

or

$$(28) \quad \ddot{u} - u^2 + 4 = \varepsilon \frac{b}{a} \dot{u} (\tau + u) + \varepsilon^2 \frac{1}{a^2} u^2 (\tau b a_1 + du) + \varepsilon^3 \frac{1}{a^2} u \dot{u} (\tau b b_1 + eu) + \mathcal{O}(\varepsilon^4).$$

The dot now indicates the derivative with respect to s . For $\varepsilon = 0$, (28) is a Hamiltonian system with the first integral,

$$(29) \quad F(u, v) := \frac{v^2}{2} + 4u - \frac{u^3}{3} = k, \quad k \in \mathbb{R}.$$

The phase portrait of (29) is presented in Figure 1. Every closed orbit of (29) surrounding $(-2, 0)$ corresponds to a level curve

$$\Gamma_k = \left\{ (u, v) \mid F(u, v) = k, \quad -\frac{16}{3} < k < \frac{16}{3} \right\},$$

and Γ_k shrinks to the equilibrium $(-2, 0)$ as $k \rightarrow -\frac{16}{3}$ and tends to a homoclinic solution as $k \rightarrow \frac{16}{3}$. The Hamiltonian system has the well-known explicit homoclinic solution $(u_0(s), v_0(s))$ given by (see, e.g., [6])

$$(30) \quad \begin{cases} u_0(s) = 2(1 - 3\operatorname{sech}^2(s)), \\ v_0(s) = 12\operatorname{sech}^2(s) \tanh(s). \end{cases}$$

This solution defines a homoclinic orbit to the saddle $(2, 0)$ (i.e., $\lim_{s \rightarrow \pm\infty} (u_0(s), v_0(s)) = (2, 0)$).

3.1. The regular perturbation method. The R-P method can be used to compute the homoclinic orbits to (28) as in [29, 30]. Assume that the homoclinic solution of (28) is parametrized by ε and approximated by

$$(31) \quad \begin{pmatrix} u(s) \\ v(s) \\ \tau \end{pmatrix} = \begin{pmatrix} u_0(s) \\ v_0(s) \\ \tau_0 \end{pmatrix} + \varepsilon \begin{pmatrix} u_1(s) \\ v_1(s) \\ \tau_1 \end{pmatrix} + \varepsilon^2 \begin{pmatrix} u_2(s) \\ v_2(s) \\ \tau_2 \end{pmatrix} + \varepsilon^3 \begin{pmatrix} u_3(s) \\ v_3(s) \\ \tau_3 \end{pmatrix} + \mathcal{O}(\varepsilon^4).$$

Inserting (31) into (28) and collecting equal powers of ε leads to the systems

$$(32) \quad \text{Order } (\varepsilon^0) : \ddot{u}_0 - u_0^2 + 4 = 0,$$

$$(33) \quad \text{Order } (\varepsilon^i) : \ddot{u}_i - 2u_0 u_i = z_i(u, v, \tau), \quad i = 1, 2, 3, \dots,$$

where $z_i(u, v, \tau)$ represent the remaining ε^i -terms which are found iteratively. The ε^0 -terms yield the Hamiltonian system with solution (30). It is not difficult to find that

$$\begin{cases} \varphi_1(s) = v_0(s), \\ \varphi_2(s) = 2 \cosh^2(s) - 15 \operatorname{sech}^2(s) (1 - s \tanh(s)) + 5 \end{cases}$$

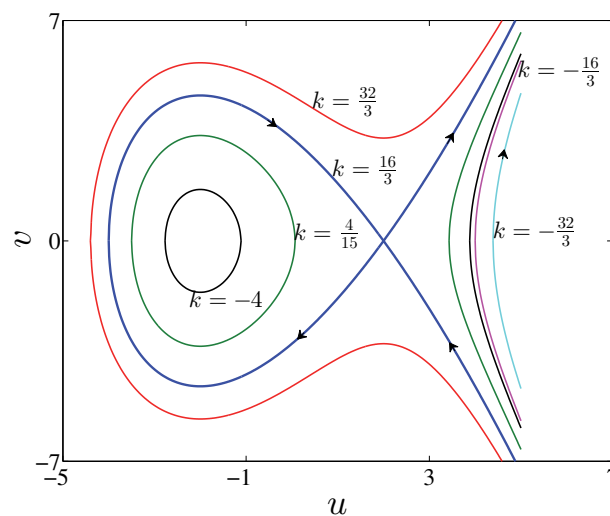


Figure 1. The phase curves of (29) for $k = \{-\frac{32}{3}, -\frac{16}{3}, -4, \frac{4}{15}, \frac{16}{3}, \frac{32}{3}\}$.

are two linearly independent solutions to the left-hand side (L.H.S.) of (33) (i.e., the homogeneous problem $\ddot{\varphi} - 2u_0\varphi = 0$) [29, 30]. Then the general solution for the inhomogeneous problem (33) can be written as

$$(34) \quad u_i(s) = \left(C_{2(i-1)+1} - \int \frac{\overbrace{\varphi_2 z_i}^{g_i}}{W(\varphi_1, \varphi_2)} dx \right) \varphi_1 + \left(C_{2(i-1)+2} + \int \frac{\overbrace{\varphi_1 z_i}^{f_i}}{W(\varphi_1, \varphi_2)} dx \right) \varphi_2,$$

$i = 1, 2, 3, \dots$, where $W(\varphi_1, \varphi_2)$ is the *Wronskian* of $\{\varphi_1, \varphi_2\}$, $C_{2(i-1)+1}$, $C_{2(i-1)+2}$ are undetermined integration constants, and $f_i(0) = g_i(0) = 0$ must hold. The description of the homoclinic solution (31) to the saddle of (28) requires that u and v be bounded (i.e., $\lim_{s \rightarrow \pm\infty} |u(s)| \neq \infty$, $\lim_{s \rightarrow \pm\infty} |v(s)| \neq \infty$), and as $s \rightarrow \pm\infty$ the solution must approach the saddle. This implies

$$\lim_{s \rightarrow \pm\infty} |u_l(s)| \neq \infty \quad \text{for } l \geq 1.$$

Under these conditions and by fixing the solution phase by requiring that [5]

$$(35) \quad v_i(0) = \dot{u}_i(0) = 0,$$

one can obtain a (unique) i th-order correction for the homoclinic solution $(u(s), v(s), \tau)$. The

second-order correction

$$(36) \quad \left\{ \begin{array}{l} \tau_0 = \frac{10}{7}, \quad \tau_1 = 0, \quad \tau_2 = \frac{4}{a} \left(\frac{25}{49} b_1 - \frac{e}{b} \right) + \frac{2}{49a^2} \left(\frac{144}{49} b^2 - 25ba_1 + 73d \right), \\ u_1(s) = -\frac{72b}{7a} \frac{\sinh(s) \log(\cosh(s))}{\cosh^3(s)}, \\ v_1(s) = -\frac{72b}{7a} \frac{\sinh^2(s) + (1 - 2\sinh^2(s)) \log(\cosh(s))}{\cosh^4(s)}, \\ u_2(s) = -\frac{216b^2}{49a^2} \frac{\log^2(\cosh(s))(\cosh(2s) - 2)}{\cosh^4(s)} - \frac{216b^2}{49a^2} \frac{\log(\cosh(s))(1 - \cosh(2s))}{\cosh^4(s)} \\ \quad - \frac{18b^2}{49a^2} \frac{(6s \sinh(2s) - 7 \cosh(2s) + 8)}{\cosh^4(s)} + \frac{(\frac{30}{7}ba_1 - 30d)}{\cosh^2(s)a^2} - \frac{2(5ba_1 + 7d)}{7a^2} \\ \quad + \frac{s(\frac{30}{7}ba_1 + 12d) \sinh(s)}{\cosh^3(s)a^2} + \frac{27d}{\cosh^4(s)a^2}, \\ v_2(s) = \dot{u}_2(s) \end{array} \right.$$

was derived in [30]. Also, a third-order correction to the Hamiltonian homoclinic solution can be explicitly given by

$$(37) \quad \left\{ \begin{array}{l} u_3(s) = \left(\left(\frac{3}{\cosh^2(s)} - 2 \right) \log(\cosh(s)) + \tanh^2(s) \right) \frac{sc_1}{\cosh^2(s)} + \frac{c_2 \tanh^3(s)}{\cosh^2(s)} \\ \quad - \left(\frac{1728b^3}{343a^3} (\log(\cosh(s))^2 - 3 \log(\cosh(s))) + c_3 \right) \frac{\sinh(s) \log(\cosh(s))}{\cosh^3(s)} \\ \quad + \left(\frac{1296b^3}{343a^3} (4 \log(\cosh(s))^2 - 7 \log(\cosh(s))) + c_4 \right) \frac{\sinh(s) \log(\cosh(s))}{\cosh^5(s)}, \\ v_3(s) = \dot{u}_3(s), \end{array} \right.$$

where

$$\begin{aligned} c_1 &= \frac{36}{343a^3} (36b^3 - 35a_1b^2 - 98bd), & c_2 &= -\frac{6}{7a^3} \left(\frac{234}{49} b^3 - 28ae + 3bd \right), \\ c_3 &= \frac{36b}{49a^3} \left(20b_1a - 25a_1b + 60d - \frac{312}{49} b^2 \right), & c_4 &= \frac{648}{7a^3} \left(bd - \frac{6}{49} b^3 \right). \end{aligned}$$

The third-order approximation (37) was not reported in [30]. Substituting (36) and (37) into (31) and then plugging the result back into (27), we obtain the third-order approximation for

the homoclinic solution of the BT normal form system (5),

$$(38) \quad \begin{cases} w_0(t) = \frac{\varepsilon^2}{a} \left(\sum_{i=0}^3 \varepsilon^i u_i(\varepsilon t) \right) + \mathcal{O}(\varepsilon^6), \\ w_1(t) = \frac{\varepsilon^3}{a} \left(\sum_{i=0}^3 \varepsilon^i v_i(\varepsilon t) \right) + \mathcal{O}(\varepsilon^7), \\ \beta_1 = -\frac{4}{a} \varepsilon^4, \\ \beta_2 = \frac{b}{a} \varepsilon^2 (\tau_0 + \varepsilon^2 \tau_2) + \mathcal{O}(\varepsilon^5). \end{cases}$$

3.2. The Lindstedt–Poincaré method. Now we apply the hyperbolic perturbation method from [10, 13, 14, 15] to improve the prediction of the homoclinic orbit in the phase space. This method is a generalized L-P method combined with hyperbolic functions instead of the Jacobian elliptic functions used in [12, 4]. We prove that this method gives the same homoclinicity conditions and then the same predictor in the parameter space. Introduce the nonlinear transformation of time,

$$(39) \quad \frac{d\xi}{ds} = \omega(\xi),$$

where $\omega(\xi)$ is a smooth bounded function, positive for all ξ . Then

$$\frac{d}{ds} = \frac{d\xi}{ds} \frac{d}{d\xi} = \omega(\xi) \frac{d}{d\xi}, \quad \frac{d^2}{ds^2} = \omega(\xi) \frac{d}{d\xi} \left(\omega(\xi) \frac{d}{d\xi} \right).$$

The new parametrization of time transforms (28) into

$$(40) \quad \omega \frac{d}{d\xi} (\omega \hat{u}') - \hat{u}^2 + 4 = \varepsilon \frac{b}{a} \omega \hat{u}' (\tau + \hat{u}) + \varepsilon^2 \frac{1}{a^2} \hat{u}^2 (\tau b a_1 + d \hat{u}) + \varepsilon^3 \frac{1}{a^2} \hat{u} \omega \hat{u}' (\tau b b_1 + e \hat{u}) + \mathcal{O}(\varepsilon^4).$$

The *hat* is used to distinguish the solution of the L-P method from the R-P solution, while the prime denotes the derivative of \hat{u} with respect to the new independent variable ξ . As before, we assume that the homoclinic solution of (40) is parametrized by ε and approximated by

$$(41) \quad \begin{pmatrix} \hat{u}(\xi) \\ \hat{v}(\xi) \\ \omega(\xi) \\ \tau \end{pmatrix} = \begin{pmatrix} \hat{u}_0(\xi) \\ \hat{v}_0(\xi) \\ \omega_0(\xi) \\ \tau_0 \end{pmatrix} + \varepsilon \begin{pmatrix} \hat{u}_1(\xi) \\ \hat{v}_1(\xi) \\ \omega_1(\xi) \\ \tau_1 \end{pmatrix} + \varepsilon^2 \begin{pmatrix} \hat{u}_2(\xi) \\ \hat{v}_2(\xi) \\ \omega_2(\xi) \\ \tau_2 \end{pmatrix} + \varepsilon^3 \begin{pmatrix} \hat{u}_3(\xi) \\ \hat{v}_3(\xi) \\ \omega_3(\xi) \\ \tau_3 \end{pmatrix} + \mathcal{O}(\varepsilon^4).$$

Substituting the series expansions (41) into (40) with $\omega_0(\xi) = 1$ ¹ and then successively collecting the terms with equal power in ε leads to the following systems:

$$(42) \quad \text{Order } (\varepsilon^0) : \hat{u}_0'' - \hat{u}_0^2 + 4 = 0,$$

$$(43) \quad \text{Order } (\varepsilon^1) : \frac{d}{d\xi} (\omega_1 \hat{u}_0') + \omega_1 \hat{u}_0'' + \hat{u}_1'' - 2\hat{u}_0 \hat{u}_1 = \frac{b}{a} \hat{u}_0' (\tau_0 + \hat{u}_0),$$

$$(44) \quad \begin{aligned} \text{Order } (\varepsilon^2) : & \frac{d}{d\xi} (\omega_2 \hat{u}_0') + \omega_2 \hat{u}_0'' + \frac{d}{d\xi} (\omega_1 \hat{u}_1') + \omega_1 \hat{u}_1'' + \hat{u}_2'' - 2\hat{u}_0 \hat{u}_2 + \omega_1 \frac{d}{d\xi} (\omega_1 \hat{u}_0') - \hat{u}_1^2 \\ & = \frac{b}{a} \hat{u}_0' (\tau_1 + \hat{u}_1) + \frac{b}{a} (\omega_1 \hat{u}_0' + \hat{u}_1') (\tau_0 + \hat{u}_0) + \frac{1}{a^2} \hat{u}_0^2 (a_1 b \tau_0 + \hat{u}_0 d), \end{aligned}$$

$$(45) \quad \begin{aligned} \text{Order } (\varepsilon^3) : & \frac{d}{d\xi} (\omega_3 \hat{u}_0') + \omega_3 \hat{u}_0'' + \frac{d}{d\xi} (\omega_2 \hat{u}_1') + \omega_2 \hat{u}_1'' + \frac{d}{d\xi} (\omega_1 \hat{u}_2') + \omega_1 \hat{u}_2'' + \hat{u}_3'' \\ & - 2\hat{u}_0 \hat{u}_3 - 2\hat{u}_2 \hat{u}_1 + \omega_2 \frac{d}{d\xi} (\omega_1 \hat{u}_0') + \omega_1 \frac{d}{d\xi} (\omega_2 \hat{u}_0') + \omega_1 \frac{d}{d\xi} (\omega_1 \hat{u}_1') \\ & = \frac{1}{a^2} (\hat{u}_0^2 (a_1 b \tau_1 + d \hat{u}_1) + 2\hat{u}_0 \hat{u}_1 (a_1 b \tau_0 + d \hat{u}_0)) \\ & + \frac{1}{a^2} \hat{u}_0' \hat{u}_0 (b b_1 \tau_0 + e \hat{u}_0) + \frac{b}{a} \hat{u}_0' (\hat{u}_2 + \tau_2) + \frac{b}{a} (\omega_1 \hat{u}_0' + \hat{u}_1') (\tau_1 + \hat{u}_1) \\ & + \frac{b}{a} (\omega_2 \hat{u}_0' + \omega_1 \hat{u}_1' + \hat{u}_2') (\tau_0 + \hat{u}_0). \end{aligned}$$

Equation (42) is identical to (28) with $\varepsilon = 0$. So it has the exact homoclinic solution

$$(46) \quad \begin{cases} \hat{u}_0(\xi) = -6\text{sech}^2(\xi) + 2, \\ \hat{v}_0(\xi) = 12\text{sech}^2(\xi) \tanh(\xi). \end{cases}$$

For $\varepsilon \neq 0$, we assume that the homoclinic solution of (40) is given by

$$(47) \quad \begin{cases} \hat{u}(\xi) = \sigma \text{sech}^2(\xi) + \delta, \\ \hat{v}(\xi) = \hat{u}'(\xi) = -2\sigma \omega(\xi) \text{sech}^2(\xi) \tanh(\xi), \end{cases}$$

where σ and δ are parameters that depend on ε ,

$$(48) \quad \begin{cases} \sigma = \sigma_0 + \varepsilon \sigma_1 + \varepsilon^2 \sigma_2 + \varepsilon^3 \sigma_3 + \mathcal{O}(\varepsilon^4), \\ \delta = \delta_0 + \varepsilon \delta_1 + \varepsilon^2 \delta_2 + \varepsilon^3 \delta_3 + \mathcal{O}(\varepsilon^4). \end{cases}$$

¹If we keep $\omega_0(\xi)$ free, then the homoclinic solution to (42) requires that $\omega_0(\xi) = 1$.

Substituting (48) into (47) and then equating each of the coefficients of ε^i to (41) yields that $\sigma_0 = -6$, $\delta_0 = 2$, and

$$(49) \quad \hat{u}_i(\xi) = \sigma_i \operatorname{sech}^2(\xi) + \delta_i, \quad i = 1, 2, 3,$$

$$(50) \quad \hat{v}_1(\xi) = \left(\omega_1(\xi) - \frac{\sigma_1}{6} \right) \hat{v}_0(\xi),$$

$$(51) \quad \hat{v}_2(\xi) = \left(\omega_2(\xi) - \frac{\sigma_1}{6} \omega_1(\xi) - \frac{\sigma_2}{6} \right) \hat{v}_0(\xi),$$

$$(52) \quad \hat{v}_3(\xi) = \left(\omega_3(\xi) - \frac{\sigma_1}{6} \omega_2(\xi) - \frac{\sigma_2}{6} \omega_1(\xi) - \frac{\sigma_3}{6} \right) \hat{v}_0(\xi).$$

Using the assumptions (49)–(52), we solve the linear equations (43)–(45) for $\hat{u}_i(\xi)$ one by one to determine τ_{i-1} , δ_i , σ_i , and $\omega_i(\xi)$ for $i = 1, 2, 3$.

We multiply both sides of (43) by \hat{u}'_0 , then integrate both sides from ξ_0 to ξ , and get

$$(53) \quad \underbrace{\int_{\xi_0}^{\xi} \hat{u}'_0 \frac{d}{dx} (\omega_1 \hat{u}'_0) dx}_{\text{I}} + \underbrace{\int_{\xi_0}^{\xi} \hat{u}'_0 \omega_1 \hat{u}''_0 dx + \int_{\xi_0}^{\xi} \hat{u}'_0 \hat{u}''_1 dx - 2 \int_{\xi_0}^{\xi} \hat{u}'_0 \hat{u}_0 \hat{u}_1 dx}_{\text{II}} = \frac{b}{a} \int_{\xi_0}^{\xi} \hat{u}_0'^2 (\tau_0 + \hat{u}_0) dx.$$

Differentiating (42) with respect to ξ , we obtain

$$(54) \quad \hat{u}_0''' = 2\hat{u}_0 \hat{u}'_0 \Rightarrow \int_{\xi_0}^{\xi} \hat{u}_1 \hat{u}_0''' dx = 2 \int_{\xi_0}^{\xi} \hat{u}_1 \hat{u}_0 \hat{u}'_0 dx.$$

The terms I and II of (53) can be simplified by

$$\begin{aligned} \text{I} &= \omega_1 \hat{u}_0'^2 \Big|_{\xi_0}^{\xi} - \cancel{\int_{\xi_0}^{\xi} \omega_1 \hat{u}'_0 \hat{u}_0'' dx} + \cancel{\int_{\xi_0}^{\xi} \omega_1 \hat{u}'_0 \hat{u}_0'' dx} = \omega_1 \hat{u}_0'^2 \Big|_{\xi_0}^{\xi}, \\ \text{II} &= (\hat{u}'_0 \hat{u}'_1 - \hat{u}_1 \hat{u}_0'') \Big|_{\xi_0}^{\xi} + \underbrace{\int_{\xi_0}^{\xi} \hat{u}_1 \hat{u}_0''' dx - 2 \int_{\xi_0}^{\xi} \hat{u}'_0 \hat{u}_0 \hat{u}_1 dx}_{\text{Using (54)}} = (\hat{u}'_0 \hat{u}'_1 - \hat{u}_1 \hat{u}_0'') \Big|_{\xi_0}^{\xi}. \end{aligned}$$

Therefore, (53) can be written as

$$(55) \quad \left(\omega_1 \hat{u}_0'^2 + \hat{u}'_0 \hat{u}'_1 - \hat{u}_1 \hat{u}_0'' \right) \Big|_{\xi_0}^{\xi} = \frac{b}{a} \int_{\xi_0}^{\xi} \hat{u}_0'^2 (\tau_0 + \hat{u}_0) dx.$$

Setting $\xi_0 = -\infty$ and $\xi = \infty$ in (55) yields the following condition for the bifurcation of homoclinic orbits:

$$\frac{b}{a} \int_{-\infty}^{\infty} \hat{u}_0'^2 (\tau_0 + \hat{u}_0) dx = 0,$$

and hence,

$$(56) \quad \frac{b}{a} \frac{192(7\tau_0 - 10)}{35} = 0 \Rightarrow \tau_0 = \frac{10}{7}.$$

Note that the same condition was derived using the classical Melnikov technique [26].

By setting $\xi_0 = 0$, $\xi = \infty$, we find that

$$(57) \quad \sigma_1 = -\delta_1.$$

We change the integration boundaries to 0 and ξ , and we get

$$(58) \quad 12\omega_1(\xi) + \delta_1 \cosh(2\xi) = -\frac{72b}{7a} \tanh(\xi).$$

Since $\omega(\xi)$ is a bounded function, we can choose the parameter δ_1 such that

$$\lim_{\xi \rightarrow \pm\infty} |\omega_1(\xi)| \neq \infty.$$

This condition implies that

$$\delta_1 = 0.$$

Thus, $\omega_1(\xi)$ is given by

$$(59) \quad \omega_1(\xi) = -\frac{6b}{7a} \tanh(\xi).$$

Substituting the values of δ_1 , σ_1 , $\omega_1(\xi)$ into (49) and (50) gives the first-order correction to the Hamiltonian homoclinic solution $(\hat{u}_0(\xi), \hat{v}_0(\xi))$,

$$(60) \quad \begin{cases} \hat{u}_1(\xi) = 0, \\ \hat{v}_1(\xi) = -\frac{6b}{7a} \tanh(\xi) \hat{v}_0(\xi). \end{cases}$$

We multiply both sides of (44) by \hat{u}'_0 and then integrate both sides from ξ_0 to ξ . Then we simplify to

$$(61) \quad \left(\omega_2 \hat{u}_0'^2 + \omega_1 \hat{u}_1'^2 + \hat{u}_0' \hat{u}_2' - \hat{u}_2 \hat{u}_0'' \right) \Big|_{\xi_0}^{\xi} + \frac{2592b^2}{49a^2} \frac{\sinh^4(x)}{\cosh^8(x)} \Big|_{\xi_0}^{\xi} = \int_{\xi_0}^{\xi} \hat{u}_0' \left(\text{R.H.S. of (44)} \right) dx.$$

We repeat the last procedure of changing the integration variables to (61) and get

$$(62) \quad \begin{cases} \tau_1 = 0, \\ \delta_2 = -\frac{2(5a_1b + 7d)}{7a^2}, \\ \sigma_2 = \frac{3}{49a^2} (70a_1b - 6b^2 - 49d), \\ \omega_2(\xi) = \frac{1}{7a^2} \left(\frac{5}{2}a_1b + \frac{18}{7}b^2 + 7d \right) - \frac{9}{4a^2} \left(\frac{6}{49}b^2 + d \right) \text{sech}^2(\xi), \end{cases}$$

with

$$(63) \quad \begin{cases} \hat{u}_2(\xi) = -\frac{3}{49a^2} (6b^2 - 70ba_1 + 49d) \text{sech}^2(\xi) - \frac{2(5a_1b + 7d)}{7a^2}, \\ \hat{v}_2(\xi) = \frac{1}{a^2} \left(\left(\frac{3}{7}b^2 - \frac{5}{14}ba_1 + \frac{3}{2}d \right) - \frac{9}{4} \left(\frac{6}{49}b^2 + d \right) \text{sech}^2(\xi) \right) \hat{v}_0(\xi). \end{cases}$$

Similarly, we multiply both sides of (45) by \hat{u}'_0 and then integrate both sides from ξ_0 to ξ . Then we simplify to

$$(64) \quad \begin{aligned} & \left(\omega_3 \hat{u}_0'^2 + \omega_2 \hat{u}_1'^2 + \omega_1 \hat{u}_2'^2 + \hat{u}_0' \hat{u}_3' - \hat{u}_3 \hat{u}_0'' \right) \Big|_{\xi_0}^{\xi} + \frac{1944}{7a^3} \left(\frac{6}{49} b^3 + bd \right) \frac{\sinh^3(x)}{\cosh^9(x)} \Big|_{\xi_0}^{\xi} \\ & - \frac{432}{7a^3} \left(\frac{36}{49} b^3 + \frac{5}{7} b^2 a_1 + 2bd \right) \frac{\sinh^3(x)}{\cosh^7(x)} \Big|_{\xi_0}^{\xi} = \int_{\xi_0}^{\xi} \hat{u}_0' \left(\text{R.H.S. of (45)} \right) dx. \end{aligned}$$

The last procedure of changing the integration variables is used to obtain

$$(65) \quad \begin{cases} \tau_2 = \frac{4}{a} \left(\frac{25}{49} b_1 - \frac{e}{b} \right) + \frac{2}{49a^2} \left(\frac{144}{49} b^2 - 25ba_1 + 73d \right), \\ \delta_3 = 0, \\ \sigma_3 = 0, \\ \omega_3(\xi) = \left(c_5 \operatorname{sech}^2(\xi) - \frac{3}{49a^3} \left(\frac{66}{49} b^3 - 20b^2 a_1 + 11bd \right) + c_6 \right) \tanh(\xi), \end{cases}$$

where

$$\begin{aligned} c_5 &= \frac{4}{a^2} e - \frac{3}{7a^3} \left(bd + \frac{6}{49} b^3 \right), \\ c_6 &= -\frac{60}{49a^2} bb_1 + \frac{3}{7a^5} \left(\frac{1}{2} bd^2 - \frac{10}{7} b^2 a_1 d + \frac{50}{49} b^3 a_1^2 + \frac{6}{49} b^3 d - \frac{60}{343} b^4 a_1 + \frac{18}{2401} b^5 \right), \end{aligned}$$

with

$$(66) \quad \begin{cases} \hat{u}_3(\xi) = 0, \\ \hat{v}_3(\xi) = \left(c_5 \operatorname{sech}^2(\xi) - \frac{18}{49a^3} \left(\frac{18}{49} b^3 - 5b^2 a_1 + 3bd \right) + c_6 \right) \tanh(\xi) \hat{v}_0(\xi). \end{cases}$$

We notice that the same values of the homoclinic bifurcation parameters $\{\tau_0, \tau_1, \tau_2\}$ were derived in [29, 30] using the R-P method. Also, the same τ_1 was derived in [5, 6] using different methods. Finally, the third-order approximation to the homoclinic orbit of the smooth BT normal form system (5) is given by

$$(67) \quad \begin{cases} w_0(t) = \frac{\varepsilon^2}{a} \left(\sum_{i=0}^3 \varepsilon^i \hat{u}_i(\xi) \right) + \mathcal{O}(\varepsilon^6), \\ w_1(t) = \frac{\varepsilon^3}{a} \left(\sum_{i=0}^3 \varepsilon^i \hat{v}_i(\xi) \right) + \mathcal{O}(\varepsilon^7), \end{cases}$$

where β_1, β_2 are the unfolding parameters as in (38).

Notice that the small displacement $\varepsilon^2 \delta_2$ in the saddle point $(2, 0)$ can be determined just by using the boundedness assumption and (40). Indeed, the saddle point is given by

$$\lim_{\xi \rightarrow \pm\infty} (\hat{u}(\xi), \hat{v}(\xi)) = (\delta, 0).$$

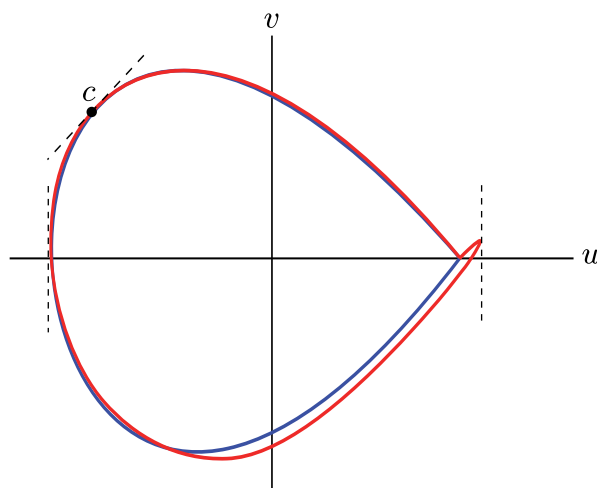


Figure 2. The “parasitic turn” near the saddle point of the homoclinic orbit predicted by (31) (red).

Since $\hat{u}'(\xi) = v(\xi)$ and $\omega(\xi)$ is a bounded function, taking the limit of both sides in (40) leads to

$$-\delta^2 + 4 = \varepsilon^2 \frac{1}{a^2} \delta^2 (\tau b a_1 + d\delta).$$

Substituting the expansions for τ and δ in this and collecting powers of ε , we get

$$\text{Order } (\varepsilon^0) : -\delta_0^2 + 4 = 0,$$

$$\text{Order } (\varepsilon^1) : -2\delta_0\delta_1 = 0,$$

$$\text{Order } (\varepsilon^2) : -2\delta_0\delta_2 - \delta_1^2 = \frac{\delta_0^2 (a_1 b \tau_0 + d\delta_0)}{a^2}.$$

We then solve at each order to get

$$\delta_0 = 2, \quad \delta_1 = 0, \quad \delta_2 = -\frac{(a_1 b \tau_0 + 2d)}{a^2},$$

with δ_2 as in (62). Note that it is only necessary to compute τ_0 to determine the ε^2 -shift of the saddle.

3.3. A comparison in the topological normal form. Consider the topological normal form (6). The homoclinic bifurcation in this system was studied in [26, 6, 39, 27, 29]. It is required that the homoclinic orbits of (6) satisfy $w_1(0) = 0$ and approach the w_0 -axis at the saddle point from both sides as $t \rightarrow \pm\infty$. Before we proceed, we check whether solutions (31) and (41) satisfy these requirements. Consider the point $c = (u(s_0), v(s_0))$, $s_0 \in (-\infty, +\infty)$, on the homoclinic orbit (we replace s by ξ and (u, v) by (\hat{u}, \hat{v}) when we talk about the homoclinic solution (41)); see Figure 2. The slope of the homoclinic orbit at a time $s = s_0$ is given by $S(s_0) = \frac{\dot{v}(s_0)}{\dot{u}(s_0)}$. The correct homoclinic orbit (the blue curve in Figure 2) can only have one vertical asymptote at time $s_0 = 0$ (i.e., where $v(0) = 0$ or, equivalently, the denominator of

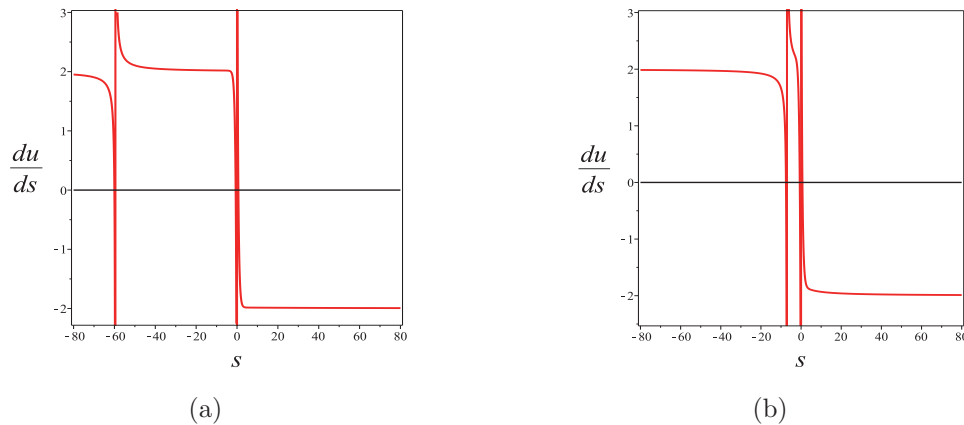


Figure 3. The asymptotes of (68) for $a = b = 1$ and (a) $\varepsilon = 0.01$, (b) $\varepsilon = 0.1$.

$S(0)$ vanishes). We can use this criterion to check whether the homoclinic solutions (31) and (41) approach the saddle point along the correct direction. Since we discuss the normal form system (6), we set $a_1 = b_1 = e = d = 0$. The homoclinic solution (41) has only one *vertical* asymptote because

$$\hat{u}'(\xi_0) = \cosh^4(\xi_0) \sinh(\xi_0) (3b^2 a^3 \varepsilon^2 + 49a^5) = 0$$

has only the trivial solution $\xi_0 = 0$ for all $\varepsilon > 0$. Moreover, the component $\hat{v}(\xi) = \sum_{i=0}^3 \varepsilon^i \hat{v}_i(\xi)$ of (41) can be written as $\hat{v}(\xi) = l(\xi) \hat{v}_0(\xi)$, where

$$l(\xi) = 1 - \varepsilon \frac{6b}{7a} \tanh(\xi) + \varepsilon^2 \frac{3b^2}{7a^2} \left(1 - \frac{9}{14} \operatorname{sech}^2(\xi) \right) - \varepsilon^3 \frac{18b^3}{343a^3} \left(\frac{3(42a^2 - b^2)}{49a^2} + \operatorname{sech}^2(\xi) \right) \tanh(\xi).$$

Then for a given (a, b) , we can always define an ε -interval such that $l(\xi) > 0$. This interval can be found by solving the inequalities $\lim_{\xi \rightarrow \pm\infty} l(\xi) > 0$ for ε (e.g., for $a = b = 1$, the function $l(\xi)$ is positive for all $\varepsilon \in [0, 1.9927)$). Thus, for this ε -interval the homoclinic solution $(\hat{u}(\xi), \hat{v}(\xi))$ intersects the \hat{u} -axis only once at $\xi = 0$ and approaches the saddle point $(-2, 0)$ from both sides as $\xi \rightarrow \pm\infty$ along the correct direction. On the other hand, for the first-order solution of (31), i.e., $u(s) = u_0(s) + \varepsilon u_1(s)$, the homoclinic orbit has two *vertical* asymptotes: one at $s_0 = 0$ and the other at the solution s_0 to

$$(68) \quad \frac{7a}{6} \sinh(s_0) \cosh(s_0) + \varepsilon \left((2 \cosh^2(s_0)b - 3b) \log(\cosh(s_0)) - \cosh^2(s_0) + b \right) = 0.$$

Figure 3a plots the L.H.S. of (68) as a function of time s_0 for $a = b = 1$ and $\varepsilon = 0.01$. It is clear that this function has a nontrivial solution at $s_0 \approx -59.52285$. This solution corresponds to the appearance of the “parasitic turn” near the saddle point (as “globally” presented in the red curve in Figure 2). Figure 3b plots (68) for $\varepsilon = 0.1$. We notice that as ε increases, the “parasitic turn” is expanding away from the saddle point, and the nontrivial zero of (68) gets closer to 0 (in general, as $\varepsilon \rightarrow 0$, the nontrivial zero of (68) $\rightarrow -\infty$ and the “parasitic turn”

shrinks to the saddle point. On the other hand, as $\varepsilon \rightarrow 1$, the nontrivial zero of (68) $\rightarrow 0$, and the “parasitic turn” grows until the homoclinic orbit breaks down). The corresponding “parasitic turn” to the numerically computed $s_0 \neq 0$ in Figure 3b is presented in Figure 4a, which plots (31) for $s \in [-16, -12.5]$ and 100,000 points, uniformly distributed. Figures 4a and 4b show the “parasitic turn” in the first- and third-order solutions of (31), respectively. Note that the visualization of the “parasitic turn” for both solutions requires a different scale. This indicates that the third-order solution provides a much more accurate solution in comparison to the first-order one. To summarize, we plot Figure 4c.

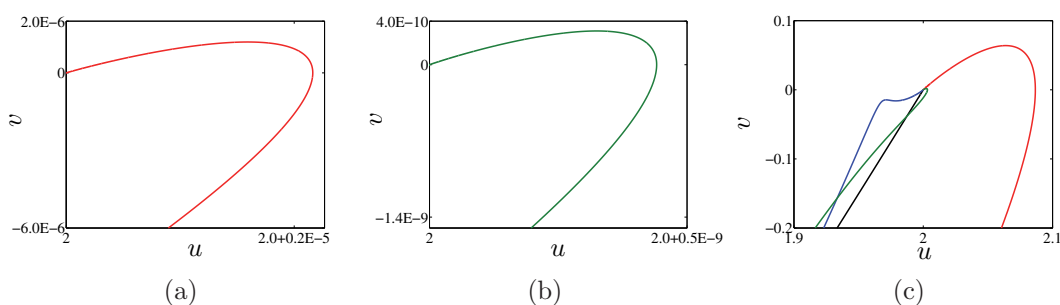


Figure 4. The “parasitic turn” for $\varepsilon = 0.1$. (a) The first-order approximation by (31). (b) The third-order approximation by (31). The “parasitic turn” of the third-order approximation is very small compared with the first-order approximation. (c) For $\varepsilon = 0.3$, the “parasitic turn” in the first-order (red), the second-order (blue), and the third-order (green) approximations by (31). The black curve denotes the third-order approximation by (41).

We return to the original problem of finding the homoclinic solution to (6). Figure 5 plots the homoclinic orbits of (6) computed with a continuation method (blue) for $a = b = 1$ and (β_1, β_2) free. At each orbit, a value of ε can be computed by taking the computed β_1 from the numerical continuation data and then solving the third equation of (38) for ε . This gives $\varepsilon = 0.139, 0.230, 0.326, 0.401, 0.470, 0.531, 0.589, 0.647, 0.707, 0.767$. Using these values of ε , we plot the corresponding homoclinic orbits obtained by (38) (red) and (67) (green). Since the bounded $\mathcal{O}(\varepsilon)$ -terms in $\omega(\xi)$ are small (see Figure 6), we approximate $\omega(\xi)$ by 1. This allows us to approximate ξ by εt . As expected, the strange behavior near the saddle point in the solution (31) is translated back to the approximate solution (38); see the close-up in Figure 5b. The orbits approach the saddle point along the “wrong” direction, making a “parasitic turn” when $t \rightarrow -\infty$ (or $t \rightarrow \infty$ for $ab < 0$) [29]. The L-P solution (i.e., (67)) has accurate orbits which nearly coincide with the computed orbits. These orbits approach the saddle point along the correct direction as $t \rightarrow \pm\infty$; i.e., near the saddle point, the strange “parasitic turn” does not appear (see Figure 5b).

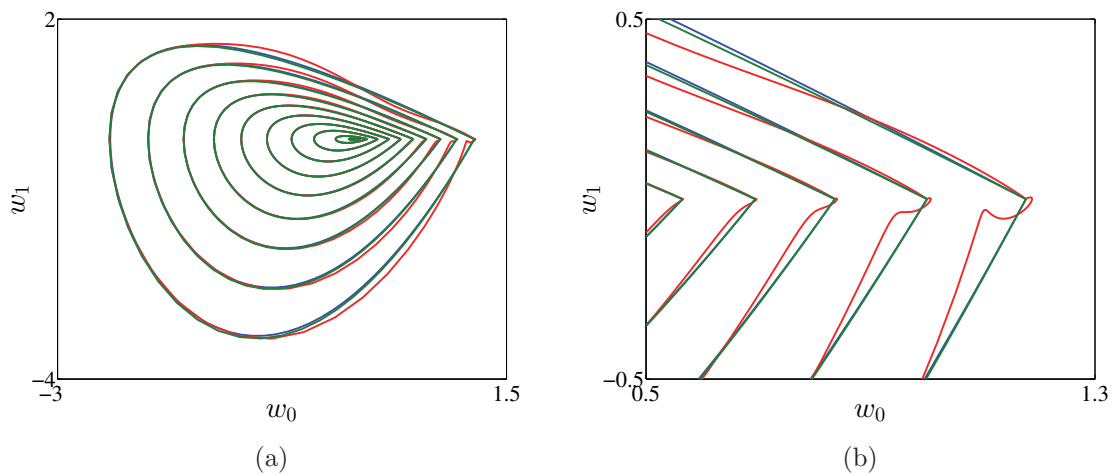


Figure 5. (a) Homoclinic orbits of (6) for $a = b = 1$ and $\varepsilon = 0.139, 0.230, 0.326, 0.401, 0.470, 0.531, 0.589, 0.647, 0.707, 0.767$. Blue orbits are computed with a continuation method, and red orbits are the homoclinic orbits approximated by the third-order truncation of (38), while green orbits are the homoclinic orbits approximated by the third-order truncation of (67). (b) Zoom of Figure 5a. For $\varepsilon \neq 0$, the approximate orbits obtained by (38) approach the saddle point along the “wrong” direction making a “parasitic turn.” This turn does not appear in the orbits obtained by (67).

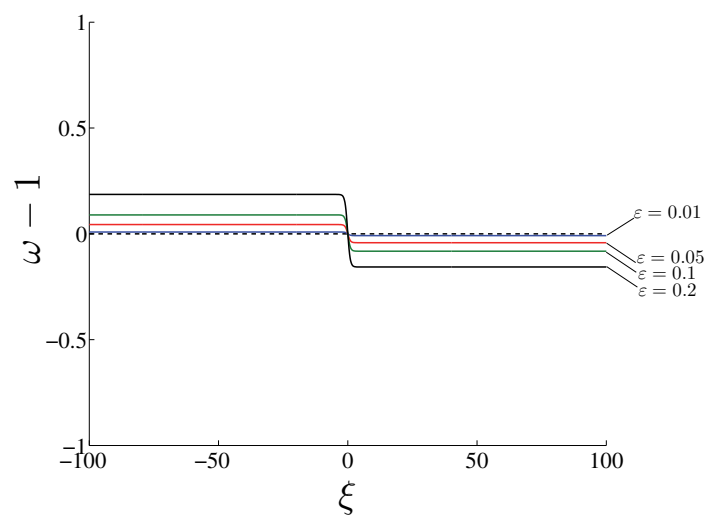


Figure 6. The computed function $\omega(\xi) - 1$ for $(a, b) = (1, 1)$ and $\varepsilon = 0.01, 0.05, 0.1, 0.2$.

4. Homoclinic asymptotics in the n -dimensional systems. In this section, we provide two explicit asymptotics for the bifurcating homoclinic orbits of (1). Following the procedure described in section 2, we transfer the BT normal form (5) with the homoclinic approximations (38) and (67) back to the original system (1). With data collected in (10b), (10c), and (11)–(26), we get two second-order homoclinic predictors x_{RP} (*the regular homoclinic asymptotic*) and x_{LP} (*Lindstedt–Poincaré homoclinic asymptotic*) for the original system (1):

(69)

$$\alpha(\varepsilon) = \frac{\varepsilon^2}{a} \frac{10b}{7} K_{1,1} + \frac{\varepsilon^4}{a} \left(-4K_{1,0} + \frac{50b^2}{49a} K_2 + b\tau_2 K_{1,1} \right) + \mathcal{O}(\varepsilon^5),$$

$$(70) \quad x_{\text{RP}}(t, \varepsilon) = \frac{\varepsilon^2}{a} \left(\frac{10b}{7} H_{0001} + u_0(s) q_0 \right) + \frac{\varepsilon^3}{a} \left(v_0(s) q_1 + u_1(s) q_0 \right) + \frac{\varepsilon^4}{a} \left(-4H_{0010} + \frac{50b^2}{49a} H_{0002} \right. \\ \left. + b\tau_2 H_{0001} + u_2(s) q_0 + v_1(s) q_1 + \frac{1}{2a} u_0^2(s) H_{2000} + \frac{10b}{7a} u_0(s) H_{1001} \right) + \mathcal{O}(\varepsilon^5),$$

$$(71) \quad x_{\text{LP}}(t, \varepsilon) = \frac{\varepsilon^2}{a} \left(\frac{10b}{7} H_{0001} + \hat{u}_0(\xi) q_0 \right) + \frac{\varepsilon^3}{a} \left(\hat{v}_0(\xi) q_1 + \hat{u}_1(\xi) q_0 \right) + \frac{\varepsilon^4}{a} \left(-4H_{0010} + \frac{50b^2}{49a} H_{0002} \right. \\ \left. + b\tau_2 H_{0001} + \hat{u}_2(\xi) q_0 + \hat{v}_1(\xi) q_1 + \frac{1}{2a} \hat{u}_0^2(\xi) H_{2000} + \frac{10b}{7a} \hat{u}_0(\xi) H_{1001} \right) + \mathcal{O}(\varepsilon^5),$$

where τ_2 is given in (36); (u_0, v_0) and (u_1, v_1, u_2) are specified by (30) and (36), respectively; and (\hat{u}_0, \hat{v}_0) , (\hat{u}_1, \hat{v}_1) , and \hat{u}_2 are specified by (46), (60), and (63), respectively.

Notice that ξ in (71) is related to $s = \varepsilon t$ by the differential equation (39). However, as explained above, we can approximate $\omega(\xi)$ by 1 and replace ξ by εt .

5. Practical initialization issues. From a numerical point of view, the continuation problem of the homoclinic orbits is well defined near but not at the BT point. So, a small nonzero step away from the BT point (essentially determined by the perturbation parameter ε) should be chosen such that the initial prediction is sufficiently close to the actual homoclinic solution. The continuation problem itself should be defined in a finite time interval instead of an infinite one. In the present section, we derive an important relation between the geometric amplitude of the homoclinic orbit and the initial perturbation parameter ε ; see Step 2 in section 5.1. We also present an extra parameter that can be used to find a suitable finite time interval where the continuation problem will converge; see Figure 7 and Step 3 in section 5.1.

In general, to continue the homoclinic orbits in two free parameters, MatCont uses an extended defining system that consists of several components (see [24, 18]).

First, the infinite time interval $[-\infty, \infty]$ is truncated to a finite interval with suitable boundary conditions, say $[-T, +T]$, where T is the half-return time. So, after applying this truncation of time, system (1) becomes

$$(72) \quad \dot{x} - 2Tf(x(t), \alpha) = 0.$$

The interval $[-T, +T]$ is rescaled to $[0, 1]$ and divided into mesh intervals where the solution is approximated by a vector polynomial of degree m (typically, $m = 4$), a linear combination

of the rescaled Lagrange basis polynomials. The mesh is nonuniform and adaptive. Each mesh interval is further subdivided by $(m + 1)$ equidistant fine mesh points and contains m collocation (Gauss) points. These points are the rescaled roots of the m th-degree Legendre polynomials [17, 27]. The numbers `ntst` of mesh intervals and `ncol` = m of collocation points are part of the continuation data chosen by the user. Equation (72) must be satisfied at each collocation point.

The second part is the equilibrium condition

$$(73) \quad f(x_0, \alpha) = 0.$$

Third, if two homoclinic parameters are free, then the following integral phase condition is added:

$$(74) \quad \int_0^1 \langle x(t) - \tilde{x}(t), \dot{\tilde{x}}(t) \rangle dt = 1,$$

where \tilde{x} is the homoclinic solution obtained at the previously found point on the curve.

Fourth, (72), (73), and (74) must be complemented with projection boundary conditions at 0 and 1,

$$(75) \quad \begin{cases} Q_S(x(0) - x_0) = 0, \\ Q_U(x(1) - x_0) = 0, \end{cases}$$

where Q_S and Q_U are matrices whose rows form a basis for the stable (S) and unstable (U) eigenspaces, respectively, of $A^T(x_0, \alpha)$. The projection boundary conditions place the solution at the two end points in the unstable and stable eigenspaces of $A(x_0, \alpha)$, respectively [9]. MatCont uses a specific algorithm that depends on the real Schur factorization and a Riccati equation to construct and update Q_S and Q_U ; for more details, see [22, 19, 23, 24, 7, 18].

Finally, the distance between $x(0)$ (respectively, $x(1)$) and x_0 must be small enough, i.e.,

$$(76) \quad \begin{cases} \varepsilon_0 = \|x(0) - x_0\|, \\ \varepsilon_1 = \|x(1) - x_0\|. \end{cases}$$

The half-return time T , ε_0 , and ε_1 are called *the homoclinic parameters*. We note that either one or two homoclinic parameters can be free.

MatCont calculates the initial homoclinic solution, the initial T , ε_0 , and ε_1 by the homoclinic predictor (71).² This is done by calling the initializer `init_BT_Hom.m` that implements *the L-P predictor* (71); then MatCont uses the initial data to start up the homoclinic continuation by calling the continuer `cont.m` which itself calls `homoclinic.m`.

5.1. The initializer `init_BT_Hom.m`. The algorithm to initialize the homoclinic continuation data proceeds as follows.

Assume that system (1) has a BT point at (x_0, α_0) .

²The predictor (70) is used in MatCont 6.1 and older versions.

Step 0. Introduce new variables, $(x, \alpha) \rightarrow (x - x_0, \alpha - \alpha_0)$, that move the BT point of (1) to the origin, $(0, 0)$.

Step 1. Compute the matrices and multilinear forms A , J_1 , B , A_1 , J_2 , C , and B_1 . Then define the nonsingular bordered system (BS) by

$$\text{BS} = \begin{pmatrix} A & w \\ v^T & 0 \end{pmatrix} \in \mathbb{R}^{(n+1) \times (n+1)}.$$

The vectors $w, v \in \mathbb{R}^n$ are chosen such that BS is nonsingular.

To compute the eigenvectors $\{q_0, q_1, p_1, p_0\} \in \mathbb{R}^n$, one starts by solving

$$\begin{aligned} \text{BS}(q_0, s) &= (0, 1), & \text{BS}(q_1, s) &= (q_0, 0), \\ \text{BS}^T(p_1, s) &= (0, 1), & \text{BS}^T(p_0, s) &= (p_1, 0). \end{aligned}$$

Following [28], these vectors are normalized by

$$\begin{aligned} \mu &= \sqrt{|q_0^T q_0|}, & q_0 &:= \frac{1}{\mu} q_0, & q_1 &:= \frac{1}{\mu} q_1, & q_1 &:= q_1 - (q_0^T q_1) q_0, \\ \nu &= q_0^T p_0, & p_1 &:= \frac{1}{\nu} p_1, & p_0 &:= p_0 - (p_0^T q_1) p_1, & p_0 &:= \frac{1}{\nu} p_0, \end{aligned}$$

and hence BS can be redefined as

$$\text{BS} = \begin{pmatrix} A & p_1 \\ q_0^T & 0 \end{pmatrix} \in \mathbb{R}^{(n+1) \times (n+1)}.$$

Step 2. Compute $a, b, H_{2000}, H_{1100}, H_{0200}, K_{1,0}, K_{1,1}, H_{0010}, H_{0001}, K_2, H_{0002}, H_{1001}, H_{0101}, d, H_{3000}, e, a_1, H_{2001}, b_1$.

Step 3. Substituting these values into (69) and (71) gives an approximation of the homoclinic solution $(x(t, \varepsilon), \alpha(\varepsilon))$. Therefore, the asymptotic homoclinic of the solution in the parameter and state space of (1) is given by $(x(t, \varepsilon), \alpha(\varepsilon)) \rightarrow (x(t, \varepsilon) + x_0, \alpha(\varepsilon) + \alpha_0)$.

Step 4. Let $A_0 := \|x(\pm\infty, \varepsilon) - x(0, \varepsilon)\|$ be the size of the initial homoclinic orbit (see Figure 7). Using (71), we approximate A_0 for small ε by

$$A_0 = \left\| \varepsilon^2 \left(\frac{2}{a} \right) q_0 - \varepsilon^2 \left(\frac{-4}{a} \right) q_0 \right\| = \varepsilon^2 \left(\frac{6}{|a|} \right).$$

The amplitude A_0 is chosen by the user, so we get

$$\varepsilon = \sqrt{A_0 \frac{|a|}{6}}.$$

This defines the initial perturbation parameter ε .

Step 5. We choose the initial T such that, at the end points, the distance

$$(77) \quad k := \|x(\pm\infty, \varepsilon) - x(\pm T, \varepsilon)\|$$

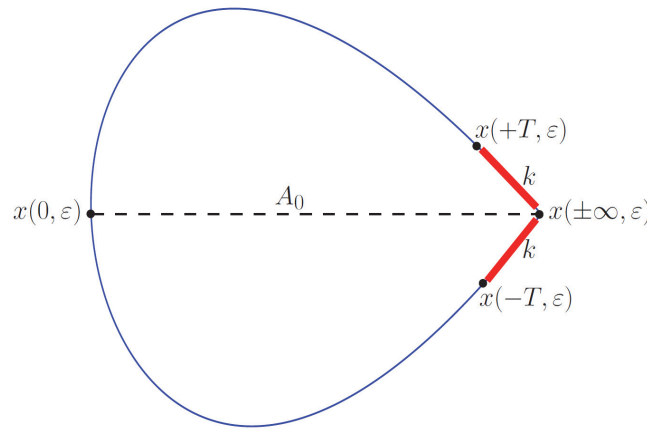


Figure 7. The initial homoclinic solution.

is sufficiently small [5]; see Figure 7. For small ε , we approximate k using (71) as

$$(78) \quad k = \varepsilon^2 \left(\frac{6\|q_0\|}{|a|} \right) \operatorname{sech}^2(\pm \varepsilon T).$$

Hence, the half-return time T can be estimated by solving $\operatorname{sech}(\varepsilon T) = \frac{1}{\varepsilon} \sqrt{\frac{k|a|}{6}}$ or, equivalently,

$$(79) \quad \operatorname{sech}(\varepsilon T) = \sqrt{\frac{k}{A_0}}.$$

The tolerance k should be small; by default it is set to 1×10^{-5} . However, in the case where a is small, we sometimes need to adjust k to find a suitable T to initialize the continuation of homoclinic orbits. This takes some trial-and-error to set k , as well as A_0 . It is possible for users to change the default values if needed in the GUI input window of MatCont (the **Starter** window; see Figure 8), where the parameters k and A_0 are denoted by **Tolerance** and **Amplitude**, respectively. Examples will be discussed in section 6.

Step 6. Compute the initial cycle by discretizing the interval $[0, 1]$ into equidistant points f_i (the *fine mesh*) and then evaluate (71) at each t , where t is given by

$$t = (2f_i - 1)T, \quad f_i \in [0, 1].$$

The initial saddle point x^* (i.e., $x(\pm\infty, \varepsilon)$) is approximated by

$$x^* = x_0 + \varepsilon^2 \left(\frac{10b}{7a} H_{0001} + \frac{2}{a} q_0 \right).$$

Step 7. From data collected in Step 3, it is now easy to compute the initial values of ε_0 and ε_1 . It is worth pointing out that $\varepsilon_{0,1}$ are computed from (71) with terms up to ε^3 . On the other hand, the value of k is computed by truncating the $\mathcal{O}(\varepsilon^3)$ from (71). So, in general k is greater than $\varepsilon_{0,1}$.

Step 8. Since all curves in MatCont are computed by a prediction-correction continuation method applied to a defining system in an appropriate discretization space \mathbb{R}^{N+1} [20], the homoclinic orbits continuation involves a calculation of the tangent vector to predict and correct the next point. If the initial point $X^i \in \mathbb{R}^{N+1}$ is sufficiently close to the homoclinic curve, then the next point in the homoclinic curve can be predicted using the initial tangent prediction

$$X^{i+1} = X^i + h_i V^i,$$

where h_i is the current step size and $V^i \in \mathbb{R}^{N+1}$ is the normalized tangent vector at the homoclinic curve at point X^i . The tangent vector at X^i is computed by solving

$$J(X^i)V^i = 0,$$

where $J(X^i) \in \mathbb{R}^{N \times (N+1)}$ is the Jacobian matrix of the defining system evaluated at X^i . The initial point can be obtained from predictor (71). Also, with data collected above for the initial homoclinic solution, one can obtain the initial tangent vector V^0 by differentiation with respect to ε . **ComputeForward** and **ComputeBackward** select the appropriate sign of V^0 without any additional computation.

6. Examples. We will use MatCont to start homoclinic orbits that emanate from BT points in two models.³ Recall that in the GUI of MatCont, k is denoted as **TTolerance**. In both models, we will set **TTolerance**= 10^{-5} . As a rule, the **Amplitude** should always be larger than **TTolerance** given the geometric meaning of both variables; cf. Figure 7. In all cases, ε_0 and ε_1 are the free homoclinic parameters since this appears to be the most stable choice. As another rule, the BT point itself should be computed to a geometric precision significantly smaller than **TTolerance**. This can be achieved in MatCont by decreasing the tolerances **VarTolerance** and **TestTolerance** for the curve on which the BT points are detected.

6.1. Indirect field oriented control system. The indirect field oriented control (IFOC) system of an induction motor is mathematically described in [2, 35] by the following ODEs:

$$(80) \quad \begin{cases} \dot{x}_1 = -c_1 x_1 + c_2 x_4 - \frac{k c_1}{u_2^0} x_2 x_4, \\ \dot{x}_2 = -c_1 x_2 + c_2 u_2^0 + \frac{k c_1}{u_2^0} x_1 x_4, \\ \dot{x}_3 = -c_3 x_3 - c_4 c_5 (x_2 x_4 - u_2^0 x_1) + (c_4 T_m + c_3 w_{ref}), \\ \dot{x}_4 = -(k_i - k_p c_3) x_3 - k_p c_4 c_5 (x_2 x_4 - u_2^0 x_1) + k_p (c_4 T_m + c_3 w_{ref}). \end{cases}$$

Here x_1, x_2, x_3 , and x_4 are the state variables, where x_1 and x_2 denote direct and quadrature components of the rotor flux; x_3 is the rotor speed error (i.e., the difference between the reference and the real mechanical speeds of the rotor); and x_4 denotes the quadrature axis component of the stator current. We also define the following constants and parameters: u_2^0 is a constant reference for the rotor flux magnitude; c_1 – c_5 are machine parameters; k_p and k_i are the proportional (P) and the integral (I) control gains, respectively; w_{ref} is the speed reference; T_m the load torque; and k is the measure of rotor time constant mismatches. The

³The examples require MatCont 6.3 or higher.

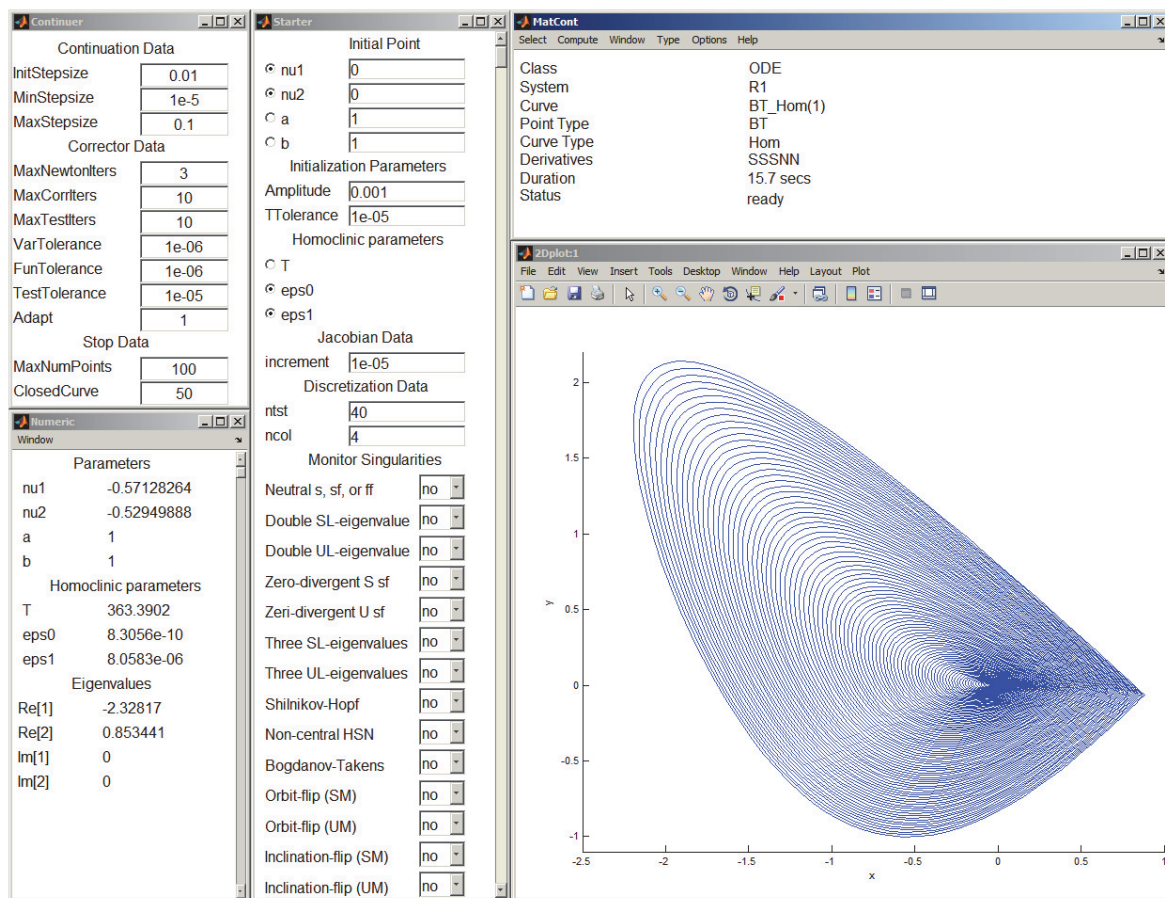


Figure 8. MatCont window during the homoclinic orbits continuation from a BT point.

occurrence of limit points (LPs) and Hopf points in IFOC has been characterized as a result of rotor time constant mismatches (see, e.g., [3, 25, 32]). The first results on the occurrence of a BT bifurcation in the IFOC model were presented in [36]. A detailed analytical study for the codim 2 bifurcations of (80) can be found in [35].

By continuation of equilibria with free k (initially $k = 17$) and fixed parameters $T_m = 5$, $c_1 = 4.4868$, $c_2 = 0.3567$, $c_3 = 0$, $c_4 = 9.743$, $c_5 = 1.911$, $u_2^0 = 11.3$, $k_p = 4.5$, $k_i = 500$, and $w_{ref} = 0$, and initial point $(x_1, x_2, x_3, x_4) = (-0.207486, 0.107263, 0, 2.534337)$, MatCont detects an LP and a Hopf point. Further, by continuation of the LP with (k, T_m) free, a BT point is detected (in Table 1 this point is labeled by BT₁). Select BT₁ and compute the Hopf curve passing through it with (k, T_m) free; an extra BT point is detected (labeled by BT₂). The smooth BT normal form coefficients at the BT points are listed in Table 2.

From the BT₂ point we start the continuation of the homoclinic curve, using k and T_m as free system parameters, $(\text{eps0}, \text{eps1})$ as free homoclinic parameters, $\text{ntst} = 40$, initial Amplitude = 2×10^{-5} , TTolerance = 1×10^{-5} , and Adapt = 1. Then **Compute|Forward**, noticing that during continuation, $T = 91.221$.

Table 1*Parameter and state values at the bifurcation points in Figure 9.*

Label	k	T_m	State variables
BT ₁	4.538573	8.109670	(−0.163289, 0.238334, 0, 10.063675)
BT ₂	4.538585	−8.109652	(0.163288, 0.238333, 0, −10.063682)

Table 2*The smooth BT normal form coefficient $\{a, b, d, e, a_1, b_1\}$ at the BT points in Figure 9.*

Label	a	b	d	e	a_1	b_1
BT ₁	28.005817	−0.911013	−4.468334	−0.435057	4.388082	0.066363
BT ₂	28.006045	−0.911099	−4.468354	−0.435062	4.388129	0.066366

For BT₁, the same procedure **Compute|Backward** can be used, noticing that during continuation, $T = 91.221$. In both cases, the initial ε is 0.01; see Figure 9.

6.2. The extended Lorenz-84 model. This example is an extended version of the Lorenz-84 model. In this model we can find all codim 2 points of equilibria (i.e., BT, CP, GH, ZH, and HH) [37, 38, 31]. Here, we discuss the switching from the BT points to the homoclinic branches. The extended Lorenz-84 model has the form

$$(81) \quad \begin{cases} \dot{X} = -Y^2 - Z^2 - \alpha X - \mu U^2 + \alpha F, \\ \dot{Y} = XY - \beta XZ - Y + G, \\ \dot{Z} = \beta XY + XZ - Z, \\ \dot{U} = -\delta U + \mu UX + S. \end{cases}$$

In this system, X models the intensity of a baroclinic wave; Y and Z are the sin and cos coefficients of the wave, respectively; and the variable U is added to study the influence of external parameters such as temperature. The parameters are fixed as follows: $\alpha = 0.25$, $\beta = 1$, $G = 0.25$, $\delta = 1.04$, $\mu = 0.987$, and $F = 2.61$.

Start the equilibria continuation with free S (initially $S = 0$) and with initial state variable values $X = 1.053698$, $Y = -0.012060$, $Z = 0.236645$, and $U = -0.580787$. Two LPs are detected. From any LP compute the LP curve passing through it with (F, S) as free system parameters. Two BT points are found (see Table 3). The smooth BT normal form coefficients at these points are listed in Table 4.

From BT₁ start the homoclinic continuation with (F, S) free, **Amplitude** = 4×10^{-5} , **TTolerance** = 1×10^{-5} , **ntst** = 40, and **Adapt** = 3, choose (**eps0**, **eps1**) as the free homoclinic parameters, then **Compute|Forward**. In the resulting continuation, $T = 1346.112$ is fixed and the initial ε is 1.2×10^{-3} . The obtained homoclinic orbits are shown in Figure 10. For BT₂ the same procedure works with **Amplitude** = 4×10^{-5} , and then **Compute|Backward** leads to a continuation with $T = 1346.112$ as well. The initial ε is 1.2×10^{-3} .

7. Conclusions. Using the smooth normal form for the codim 2 Bogdanov–Takens (BT) bifurcation on the center manifold, we derived for the first time the explicit third-order

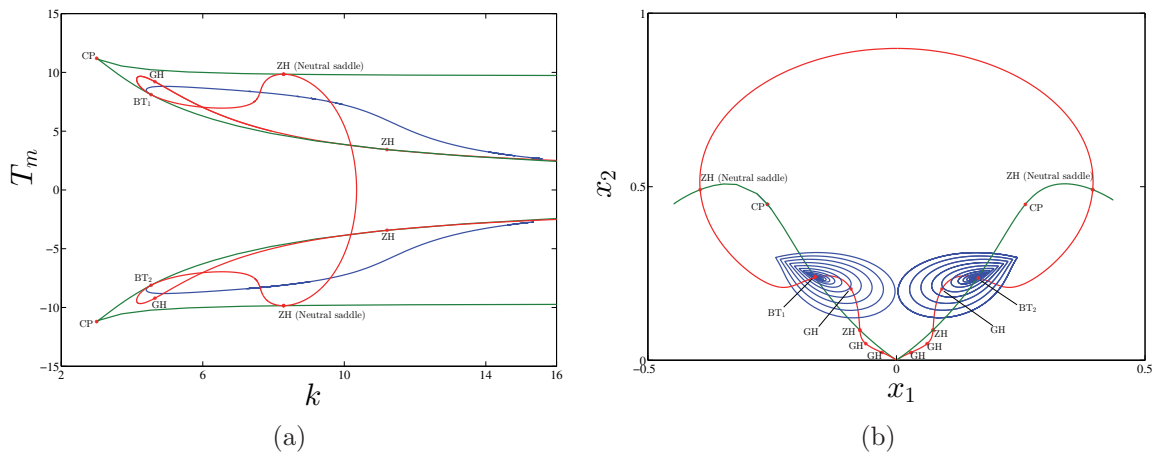


Figure 9. Continuation of the homoclinic orbits emanating from the BT points of the IFOC model with (k, T_m) free. The blue curve is the homoclinic orbit, the green is the LP curve, and the red is the Hopf curve. (a) The homoclinic orbits in parameter space (k, T_m) . (b) The homoclinic orbits in state space (x_1, x_2) .

Table 3

Parameter and state values at the bifurcation points in Figure 10.

Label	F	S	State variables
BT ₁	1.446717	0.020940	(1.225641, -0.036321, 0.197288, -0.123390)
BT ₂	1.446722	-0.020941	(1.225646, -0.036321, 0.197287, 0.123392)

Table 4

The smooth BT normal form coefficients $\{a, b, d, e, a_1, b_1\}$ at the BT points in Figure 10.

Label	a	b	d	e	a_1	b_1
BT ₁	0.214424	0.606515	-0.2381464	-2.815244	0.588486	1.238143
BT ₂	0.214426	0.606525	-0.2381432	-2.815177	0.588481	1.238118

homoclinic predictors applying both the regular (R-P) and the Lindstedt–Poincaré (L-P) perturbation methods. Both methods give the same asymptotic for the homoclinic parameter values. However, the L-P predictor has a clear advantage, since it does not suffer from the “parasitic turn” in the asymptotic for the homoclinic orbit in the phase space. Recall that the order of predictor refers to the maximal order in the ε -expansion of the homoclinic solution in the perturbed Hamiltonian systems, and not to the truncation ε -order in the final predictors.

The L-P method for standard oscillators removes secular terms; i.e., a linear time-rescaling depending on the small parameter ε yields a choice to eliminate unbounded terms and allows us to obtain a solution valid for all time. Then an expansion in ε recovers the unbounded term. Here we argue that our homoclinic predictor obtained from the L-P method is related in a similar way to the predictor from the R-P method. The difference, however, is that here we remove the parasitic turns rather than the secular terms. Our claim is that if we expand

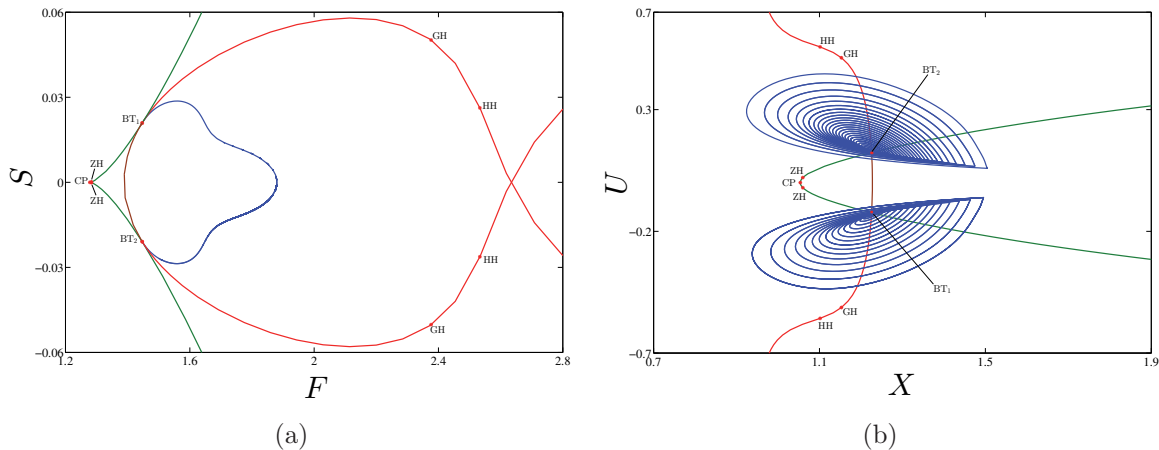


Figure 10. Continuation of the homoclinic orbits emanating from the BT points of the Lorenz-84 model with (F, S) free. The blue curve is the homoclinic orbit, the green is the LP curve, the red is the Hopf curve, and the brown is a neutral-saddle curve. (a) Homoclinic orbits in parameter space. (b) Homoclinic orbits in (X, U) -space.

the L-P predictor including the ε -dependent rescaled time, we recover the R-P predictor in the corresponding order. This implies that the geometry of the predictor is correct in phase space. We will restrict ourselves to first order in ε . First, from (59) we have

$$\frac{d\xi}{ds} = 1 - \varepsilon \frac{6b}{7a} \tanh(\xi) + O(\varepsilon^2) \implies \frac{ds}{d\xi} = 1 + \varepsilon \frac{6b}{7a} \tanh(\xi) + O(\varepsilon^2),$$

which can be integrated and inverted to yield

$$s = \xi + \varepsilon \frac{6b}{7a} \log(\cosh(\xi)) + O(\varepsilon^2) \implies \xi = s - \varepsilon \frac{6b}{7a} \log(\cosh(s)) + O(\varepsilon^2).$$

Then it is easily checked that $u_{0,LP}(\xi(s)) = u_{0,RP}(s) + \varepsilon u_{1,RP}(s) + O(\varepsilon^2)$ and that $v_{0,LP}(\xi(s)) + \varepsilon v_{1,LP}(\xi(s)) = v_{0,RP}(s) + \varepsilon v_{1,RP}(s) + O(\varepsilon^2)$. The parasitic turn appears due to the log-term, so it is present in the R-P predictor. In the L-P predictor, this turn is removed by a nonlinear time reparametrization along the homoclinic orbit. We conjecture that this holds for higher order terms in ε as well. Note that for the L-P method we prescribe the u -solution, restricting the homoclinic excursion to one side of the saddle point. Then solvability requires additional freedom, provided by the time-rescaling. For the R-P method the solution satisfies $\dot{u} = v$, which by the time-rescaling does not hold in the L-P method. Also, for large values of ε , $d\xi/ds$ may become negative, marking the end of the validity of the asymptotic.

We have described an initializer implemented in MatCont to start homoclinic orbits from a BT point based on the L-P perturbation method. The initializer allows us to compute the initial homoclinic solution and parameters so that the continuation of the homoclinic orbit can be started. We suggest allowing `eps0` and `eps1` to vary as homoclinic parameters and to set `TTolerance` = 1×10^{-5} . In the MatCont **Continuer** window, set **Adapt** = 1. Then start to increase/decrease the **Amplitude** value. This works for most studied models. However,

this choice is not an absolute rule, and it takes some trial-and-error to set all parameters (including **TTolerance**, continuation parameters, and adaptation (**Adapt**)) for the successful continuation. Note that in each case, both **Compute|Forward** and **Compute|Backward** should be tried. In general, cases where a has small (absolute) value are more difficult to handle than cases where a is moderate.

REFERENCES

- [1] V. I. ARNOLD, *Geometrical Methods in the Theory of Ordinary Differential Equations*, Springer-Verlag, New York, Heidelberg, Berlin, 1983.
- [2] A. S. BAZANELLA AND R. REGINATTO, *Robustness margins for indirect field oriented control of induction motors*, IEEE Trans. Automat. Control, 45 (2000), pp. 1226–1231.
- [3] A. S. BAZANELLA AND R. REGINATTO, *Instability mechanisms in indirect field oriented control drives: Theory and experimental results*, in Proceedings of the 15th IFAC World Congress (Barcelona, Spain), IFAC Proc. Vol. 15, Elsevier, Amsterdam, 2002, pp. 125–130. <http://dx.doi.org/10.3182/20020721-6-ES-1901.01574>.
- [4] M. BELHAQ, B. FIEDLER, AND F. LAKRAD, *Homoclinic connections in strongly self-excited nonlinear oscillators: The Melnikov function and the elliptic Lindstedt-Poincaré method*, Nonlinear Dynam., 23 (2000), pp. 67–86.
- [5] W.-J. BEYN, *Numerical analysis of homoclinic orbits emanating from a Takens-Bogdanov point*, IMA J. Numer. Anal., 14 (1994), pp. 381–410.
- [6] W.-J. BEYN, A. CHAMPNEYS, E. J. DOEDEL, W. GOVAERTS, YU. A. KUZNETSOV, AND B. SANDSTEDE, *Numerical continuation, and computation of normal forms*, in Handbook of Dynamical Systems, Vol. 2, B. Fiedler, ed., North-Holland, Amsterdam, 2002, pp. 149–219.
- [7] S. BINDEL, J. DEMMEL, AND M. FRIEDMAN, *Continuation of Invariant Subspaces for Large Bifurcation Problems*, Tech. Report UCB/EECS-2006-13, EECS Department, University of California, Berkeley, 2006.
- [8] Y. Y. CAO, K. W. CHUNG, AND J. XU, *A novel construction of homoclinic and heteroclinic orbits in nonlinear oscillators by a perturbation-incremental method*, Nonlinear Dynam., 64 (2011), pp. 221–236.
- [9] A. R. CHAMPNEYS, YU. A. KUZNETSOV, AND B. SANDSTEDE, *A numerical toolbox for homoclinic bifurcation analysis*, Internat. J. Bifur. Chaos Appl. Sci. Engrg., 6 (1996), pp. 867–887.
- [10] S. H. CHEN, Y. Y. CHEN, AND K. Y. SZE, *A hyperbolic perturbation method for determining homoclinic solution of certain strongly nonlinear autonomous oscillators*, J. Sound Vibration, 322 (2009), pp. 381–392.
- [11] S. H. CHEN, Y. Y. CHEN, AND K. Y. SZE, *Homoclinic and heteroclinic solutions of cubic strongly nonlinear autonomous oscillators by hyperbolic Lindstedt-Poincaré method*, Sci. China Technol. Sci., 53 (2010), pp. 692–702.
- [12] S. H. CHEN, X. M. YANG, AND Y. K. CHEUNG, *Periodic solutions of strongly quadratic non-linear oscillators by the elliptic Lindstedt-Poincaré method*, J. Sound Vibration, 212 (1998), pp. 771–780.
- [13] Y. Y. CHEN AND S. H. CHEN, *Homoclinic and heteroclinic solutions of cubic strongly nonlinear autonomous oscillators by the hyperbolic perturbation method*, Nonlinear Dynam., 58 (2009), pp. 417–429.
- [14] Y. Y. CHEN, S. H. CHEN, AND K. Y. SZE, *A hyperbolic Lindstedt-Poincaré method for homoclinic motion of a kind of strongly nonlinear autonomous oscillators*, Acta Mech. Sin., 25 (2009), pp. 721–729.
- [15] Y. Y. CHEN, L. W. YAN, K. Y. SZE, AND S. H. CHEN, *Generalized hyperbolic perturbation method for homoclinic solutions of strongly nonlinear autonomous systems*, Appl. Math. Mech. (English Ed.), 33 (2012), pp. 1137–1152.
- [16] S.-N. CHOW, C. LI, AND D. WANG, *Normal Forms and Bifurcation of Planar Vector Fields*, Cambridge University Press, Cambridge, UK, 1994.
- [17] C. DE BOOR AND B. SWARTZ, *Collocation at Gaussian points*, SIAM J. Numer. Anal., 10 (1973), pp. 582–606. <http://epubs.siam.org/doi/abs/10.1137/0710052>.

- [18] V. DE WITTE, W. GOVAERTS, YU. A. KUZNETSOV, AND M. FRIEDMAN, *Interactive initialization and continuation of homoclinic and heteroclinic orbits in MATLAB*, ACM Trans. Math. Software, 38 (2012), 18 (34 pages).
- [19] J. W. DEMMEL, L. DIECI, AND M. J. FRIEDMAN, *Computing connecting orbits via an improved algorithm for continuing invariant subspaces*, SIAM J. Sci. Comput., 22 (2000), pp. 81–94. <http://epubs.siam.org/doi/abs/10.1137/S1064827598344868>.
- [20] A. DHOOGHE, W. GOVAERTS, AND YU. A. KUZNETSOV, *MATCONT: A MATLAB package for numerical bifurcation analysis of ODEs*, ACM Trans. Math. Software, 29 (2003), pp. 141–164.
- [21] A. DHOOGHE, W. GOVAERTS, YU. A. KUZNETSOV, H. G. E. MEIJER, AND B. SAUTOIS, *New features of the software MatCont for bifurcation analysis of dynamical systems*, Math. Comput. Model. Dyn. Syst., 14 (2008), pp. 147–175.
- [22] L. DIECI AND T. EIROLA, *On smooth decompositions of matrices*, SIAM J. Matrix Anal. Appl., 20 (1999), pp. 800–819. <http://epubs.siam.org/doi/abs/10.1137/S0895479897330182>.
- [23] L. DIECI AND M. FRIEDMAN, *Continuation of invariant subspaces*, Numer. Linear Algebra Appl., 8 (2001), pp. 317–327.
- [24] M. FRIEDMAN, W. GOVAERTS, YU. A. KUZNETSOV, AND B. SAUTOIS, *Continuation of homoclinic orbits in MATLAB*, in Computational Science (ICCS 2005), Lecture Notes in Comput. Sci. 3514, V. S. Sunderam, G. D. van Albada, P. M. A. Sloot, and J. J. Dongarra, eds., Springer, Berlin, Heidelberg, 2005, pp. 263–270.
- [25] F. GORDILLO, F. SALAS, R. ORTEGA, AND J. ARACIL, *Hopf bifurcation in indirect field-oriented control of induction motors*, Automatica, 38 (2002), pp. 829–835.
- [26] J. GUCKENHEIMER AND P. HOLMES, *Nonlinear Oscillations, Dynamical Systems and Bifurcations of Vector Fields*, Springer-Verlag, New York, 1983.
- [27] YU. A. KUZNETSOV, *Elements of Applied Bifurcation Theory*, 3rd ed., Springer-Verlag, New York, 2004.
- [28] YU. A. KUZNETSOV, *Practical computation of normal forms on center manifolds at degenerate Bogdanov-Takens bifurcations*, Internat. J. Bifur. Chaos Appl. Sci. Engrg., 15 (2005), pp. 3535–3546.
- [29] YU. A. KUZNETSOV, H. G. E. MEIJER, B. AL-HDAIBAT, AND W. GOVAERTS, *Improved homoclinic predictor for Bogdanov-Takens bifurcation*, Internat. J. Bifur. Chaos Appl. Sci. Engrg., 24 (2014), 1450057 (12 pages).
- [30] YU. A. KUZNETSOV, H. G. E. MEIJER, B. AL-HDAIBAT, AND W. GOVAERTS, *Accurate approximation of homoclinic solutions in Gray-Scott kinetic model*, Internat. J. Bifur. Chaos Appl. Sci. Engrg., 25 (2015), 1550125 (10 pages).
- [31] YU. A. KUZNETSOV, H. G. E. MEIJER, W. GOVAERTS, AND B. SAUTOIS, *Switching to nonhyperbolic cycles from codim 2 bifurcations of equilibria in ODEs*, Phys. D, 237 (2008), pp. 3061–3068.
- [32] J. MOIOLA AND G. CHEN, *Hopf Bifurcation Analysis: A Frequency Domain Approach*, World Scientific, Singapore, 1996.
- [33] A. H. NAYFEH, *Introduction to Perturbation Techniques*, John Wiley & Sons, New York, 1981.
- [34] A. J. RODRÍGUEZ-LUIS, E. FREIRE, AND E. PONCE, *A method for homoclinic and heteroclinic continuation in two and three dimensions*, in Continuation and Bifurcations: Numerical Techniques and Applications, NATO Adv. Sci. Inst. Ser. C Math. Phys. Sci. 313, D. Roose, B. De Dier, and A. Spence, eds., Kluwer Acad. Publ., Dordrecht, 1990, pp. 197–210.
- [35] F. SALAS, F. GORDILLO, AND J. ARACIL, *Codimension-two bifurcations in indirect field oriented control of induction motor drives*, Internat. J. Bifur. Chaos Appl. Sci. Engrg., 18 (2008), pp. 779–792.
- [36] F. SALAS, R. REGINATTO, F. GORDILLO, AND J. ARACIL, *Bogdanov-Takens bifurcation in indirect field oriented control of induction motor drives*, in Proceedings of the 43rd IEEE Conference on Decision and Control (Atlantis, Bahamas), Vol. 4, IEEE, Piscataway, NJ, 2004, pp. 4357–4362. <http://ieeexplore.ieee.org/xpl/articleDetails.jsp?arnumber=1429436>.
- [37] A. SHIL'NIKOV, G. NICOLIS, AND C. NICOLIS, *Bifurcation and predictability analysis of a low-order atmospheric circulation model*, Internat. J. Bifur. Chaos Appl. Sci. Engrg., 5 (1995), pp. 1701–1711.
- [38] L. VAN VEEN, *Baroclinic flow and the Lorenz-84 model*, Internat. J. Bifur. Chaos Appl. Sci. Engrg., 13 (2003), pp. 2117–2139.
- [39] S. WIGGINS, *Introduction to Applied Nonlinear Dynamical Systems and Chaos*, 2nd ed., Springer-Verlag, New York, 2003.